Mitigation of Almond Leaf Scorch by a Peptide that Inhibits the Motility of *Xylella fastidiosa*

Luis Moll,[1] Esther Badosa,[1] Leonardo De La Fuente,[2] Emilio Montesinos,[1] Marta Planas,[3] Anna Bonaterra,[1,†] and Lidia Feliu[3,†]

[1] Laboratory of Plant Pathology, Institute of Food and Agricultural Technology-CIDSAV, Campus Montilivi, University of Girona, 17003 Girona, Spain
[2] Department of Entomology and Plant Pathology, Auburn University, Auburn, AL 36849, U.S.A.
[3] LIPPSO, Department of Chemistry, Campus Montilivi, University of Girona, 17003 Girona, Spain

Abstract

Xylella fastidiosa is a xylem-limited plant pathogenic bacterium that is a menace to the agriculture worldwide, threating economically relevant crops such as almond. The pathogen presents a dual lifestyle in the plant xylem, consisting of sessile microbial aggregates and mobile independent cells that move by twitching motility. The latter is essential for the systemic colonization of the host and is mediated through type IV pili. In previous reports, it has been demonstrated that peptides can affect different key processes of *X. fastidiosa*, but their effect on motility has never been assessed. In the present work, peptides previously identified and newly designed analogs were studied for their effect in vitro on the motility of *X. fastidiosa*, and their protective effect against almond leaf scorch was determined. By assessing the twitching fringe width in colonies and using microfluidic chambers, the inhibitory effect of BP100 on twitching motility was demonstrated. Interestingly, type IV pili of BP100-treated cells were similar in frequency and length and presented no morphological differences when compared with the nontreated control. The application of BP100 by endotherapy in almond plants inoculated with *X. fastidiosa* under greenhouse conditions significantly reduced population levels and showed less affected xylem vessels, which correlated with decreased disease symptoms. Therefore, BP100 is a promising candidate to manage almond leaf scorch caused by *X. fastidiosa*.

Keywords: motility, synthetic antimicrobial peptides, twitching inhibition, type IV pili, *Xylella fastidiosa*

Xylella fastidiosa is a gram-negative, xylem-limited, vector-transmitted bacterium that poses a great threat to agriculture worldwide because it can infect more than 600 plant taxa. The bacterium is responsible of economically severe crop diseases such as Pierce's disease, citrus variegated chlorosis, olive quick decline syndrome and almond leaf scorch (ALS) (Alston et al. 2013; Baró et al. 2021; Purcell 2013; Rapicavoli et al. 2018). The pathogen was introduced into the European Union (EU) and is spreading through the Mediterranean region with the potential to affect the agricultural economy of countries that are global producers of olives, citrus, almonds, and grapes, such as Italy, Spain, France, and Greece (Choueiri et al. 2023; European Food Safety Authority 2013; European Food Safety Authority et al. 2023; Strona et al. 2017). In fact, the potential economic losses associated to the full spread of *X. fastidiosa* in the EU have been estimated to be 5.5 billion Euros per year and has been ranked as a priority quarantine pathogen in the area (Sánchez et al. 2019). Most of the measures adopted to manage diseases caused by *X. fastidiosa* are focused on eradication, limiting the spread of the bacterium by controlling its vector, and replacing susceptible varieties with tolerant ones (Anita et al. 2022; Avosani et al. 2024; Carluccio et al. 2023; EFSA Panel on Plant Health et al. 2019; Matsumoto et al. 2023). Other approaches that are under study are based on the reduction of the pathogen population in infected plants by using the endophyte *Paraburkholderia phytofirmans* (Baccari et al. 2019; Lindow et al. 2024), avirulent *X. fastidiosa* strains (Hao et al. 2017), lytic phages (Das et al. 2015; Stefani et al. 2021), and chemical compounds such as copper (II) compounds (Ge et al. 2020), a zinc, copper and citric acid biocomplex (Scortichini et al. 2018), antibiotics (Amanifar et al. 2016) and N-acetyl-L-cysteine (Muranaka et al. 2013). Although considerable research has been performed, there is still no strategy to protect and completely cure infected plants (Burbank 2022).

Peptides with antimicrobial activity against *X. fastidiosa* have been reported, including cecropin B, magainin 2, and indolicidin (Fogaça et al. 2010; Kuzina et al. 2006; Li and Gray 2003; Montesinos 2023). In recent studies, we have identified other antimicrobial peptides active in vitro and in vivo against *X. fastidiosa* (Badosa et al. 2022). For example, BP178 showed bactericidal activity in vitro (Baró et al. 2020a, b) and caused a significant disease control when applied in infected almond plants by endotherapy, which consists of precisely introducing the peptide directly into the vascular system by injection (Moll et al. 2022). Peptides 1036 and RIJK2 also exhibited high bactericidal and antibiofilm activity against *X. fastidiosa* (Moll et al. 2021). These studies demonstrate that peptides that affect different key processes of *X. fastidiosa*, could be considered as promising candidates to control the diseases that it causes.

X. fastidiosa presents a dual lifestyle consisting of mobile independent cells (planktonic) and sessile microbial aggregates (biofilm) that switch depending on environmental conditions (Beaulieu et al. 2013; Cardinale et al. 2018; Chatterjee et al. 2010). Planktonic cells are able to systemically colonize the plant upstream and downstream from the initial site of infection by moving with and against the xylem sap flow (Pereira et al. 2019; Shi and Lin 2016). This bacterium lacks flagella but possesses type IV pili that allow cells to migrate using a type of movement known as twitching (Li et al. 2007; Meng et al. 2005). Type IV pili are filamentous appendages mostly found at one pole of the cells that consist of pilin

[†]Corresponding authors: A. Bonaterra; anna.bonaterra@udg.edu, and L. Feliu; lidia.feliu@udg.edu

Funding: This work was supported by grants from the European Commission BeXyL (grant 101060593, HORIZON EUROPE Food, Bioeconomy, Natural Resources, Agriculture and Environment) and from the Spain Ministerio de Ciencia e Innovación (MCIU)/Agencia Estatal de Investigación and EU FEDER (TED2021-130110B-C43, PID2022-140040OB-C21 and C22). L. Moll was a recipient of a research grant from Spain MCIU (Ref. FPU19/01434 and EST22/00007).

***e*-Xtra:** Supplementary material is available online.

The author(s) declare no conflict of interest.

Accepted for publication 4 September 2024.

subunits that are polymerized into a filamentous structure extruded from the cell (De La Fuente et al. 2007b; Li et al. 2007; Meng et al. 2005; Román-Écija et al. 2023). Once it attaches to a surface, the depolymerization of the structure is induced, resulting in a pulling motion (Kaiser 2000). This process is modulated by a complex protein machinery that spans from the inner to the outer cell membrane of the pathogen (Craig et al. 2019; Dunger et al. 2016).

Apart from being responsible for the movement of the bacteria, type IV pili are involved in other important functions such as adhesion and biofilm formation, as well as natural competence by internalization of genetic material from the environment (Jacobsen et al. 2020; Merfa et al. 2023) and are crucial in the development of diseases caused by *X. fastidiosa*. Therefore, alterations in their functionality result in delayed and less severe symptoms in planta (Chatterjee et al. 2008b; Cruz et al. 2014; Cursino et al. 2011).

Peptides, such as 1037 and Cec4, and other compounds, such as zingerone, affect the motility of gram-negative bacterial pathogens, such as *Acinetobacter baumannii* and *Pseudomonas aeruginosa* (de la Fuente-Núñez et al. 2012; Dong et al. 2019; Kumar et al. 2013; Liu et al. 2020; Shang et al. 2021). Nevertheless, as far as we know, the effect of peptides on the motility of *X. fastidiosa* has never been evaluated (Chatterjee et al. 2008b; Roper et al. 2019). Only calcium, copper, zinc, oxylipins, and bovine serum albumin (BSA) have been described to interfere with the motility of the pathogen (Chen and De La Fuente 2020; Cobine et al. 2013; Cruz et al. 2012; Galvani et al. 2007; Scala et al. 2020). In particular, media supplemented with calcium caused an increase in twitching motility under microfluidic chamber conditions, and BSA prevented fringe formation on colonies of *X. fastidiosa* (Cruz et al. 2012; Galvani et al. 2007). Therefore, we set out to determine whether peptides can alter the twitching motility of *X. fastidiosa* and disease development.

The aim of the present work was to identify peptides that interfere with the motility of *X. fastidiosa* and to determine their efficacy in reducing disease severity caused by this bacterium. Firstly, the cell motility of several *X. fastidiosa* strains was determined to choose the appropriate strain to evaluate the activity of the peptides on its motility. Secondly, a set of peptides was synthesized and characterized for their bactericidal and antibiofilm activity, their effect on leaf infiltration in a tobacco plant model, and their hemolytic activity to select candidates to study their effect on the motility of *X. fastidiosa*. Finally, the most active peptides were tested in almond plant assays to determine their effect on population levels and disease development under greenhouse conditions.

Materials and Methods

Selection, design, and synthesis of peptides

This work was centered on identifying peptides that influence the motility of *X. fastidiosa* (Table 1). The selected peptides were: (i) 1036, RIJK2, BP100, HP1404-T1E, FV7, and R-FV7-I16, with bactericidal or antibiofilm activity against *X. fastidiosa* (Baró et al. 2020a; Moll et al. 2021); (ii) KSLW and BP16, sequences with antibiofilm activity against gram-negative bacteria or low toxicity (Badosa et al. 2007; Camó et al. 2019; Gawande et al. 2014); and (iii) new modified peptides based on the sequences of peptides mentioned above. The latter were designed by conjugating FV7 at the N- or C-terminus of BP100, BP16, and KSLW (FV7-BP100, BP100-FV7, FV7-BP16, BP16-FV7, FV7-KSLW, KSLW-FV7) and by replacing specific amino acids of 1036. In particular, arginine residues of 1036 were substituted by lysines (BP534), the phenylalanine was replaced by a tryptophan (BP535), or the glutamine was replaced by an arginine (BP536). In addition, BP178 was included as a reference peptide in the plant experiments (Baró et al. 2020a; Moll et al. 2022; Montesinos et al. 2021).

Peptides (Supplementary Table S1) were synthesized manually on solid phase using standard 9-fluorenylmethoxycarbonyl

Table 1. Sequences of the peptides and their previously described activities

Code[a]	Sequence[b]	Described activity[c]		References
		Antibacterial	Antibiofilm	
FV7	FRIRVRV-NH_2	*Ec, Pa, Se, Sp*	*Ec, Pa, Xf*	Moll et al. 2021; Xu et al. 2014
BP100	KKLFKKILKYL-NH_2	*Ea, Pss, Psa, Xap, Xav, Xf*	*Pa*	Ajish et al. 2022; Badosa et al. 2007; Baró et al. 2020a
BP16	KKLFKKILKKL-NH_2	*Ea, Pss, Psa, Xap, Xav*	nd	Badosa et al. 2007; Caravaca-Fuentes et al. 2021
KSLW	KKVVFWVKFK-NH_2	*Aa, Ea, Pss, Psa, Xap, Xav*	Oral biofilms	Camó et al. 2019; Na et al. 2007
FV7-BP100	FRIRVRV-KKLFKKILKYL-NH_2	–	–	This work
BP100-FV7	KKLFKKILKYL-FRIRVRV-NH_2	–	–	This work
FV7-BP16	FRIRVRV-KKLFKKILKKL-NH_2	–	–	This work
BP16-FV7	KKLFKKILKKL-FRIRVRV-NH_2	–	–	This work
FV7-KSLW	FRIRVRV-KKVVFWVKFK-NH_2	–	–	This work
KSLW-FV7	KKVVFWVKFK-FRIRVRV-NH_2	–	–	This work
1036	VQFRIRVRIVIRK-NH_2	*Pa, Bc, Xf*	*Pa, Bc, Xf*	de la Fuente-Núñez et al. 2012; Moll et al. 2021
BP534	VQF**K**I**K**V**K**IVI**KK**-NH_2	–	–	This work
BP535	VQ**W**RIRVRIVIRK-NH_2	–	–	This work
BP536	V**R**FRIRVRIVIRK-NH_2	–	–	This work
RIJK2	RIVWVRIRRWFV-NH_2	*Xf*	*Pa, Kp, Xf*	de la Fuente-Núñez et al. 2015; Moll et al. 2021
HP1404 T1-E	IL**K**KL**L**KKVK**K**I-NH_2	*Pa*	*Pa, Xf*	Kim et al. 2018; Moll et al. 2021
R-FV7-I16	RFRRL-FRIRVRV-LKKI-NH_2	*Ec, Pa, Se*	*Ec, Pa, Xf*	Moll et al. 2021; Xu et al. 2014
BP178	KKLFKKILKYLAGPA-GIGKFLHSAKKDE-OH	*Xf, Xav, Pto*	nd	Baró et al. 2020b; Moll et al. 2022; Montesinos et al. 2021

[a] Highlighted peptides correspond to previously described ones.

[b] Underlined amino acids correspond to their D isomer. Bold-marked amino acids indicate the amino acid substitutions performed when compared with the parental sequence.

[c] Only activities described against gram-negative bacteria are taken into consideration. *Aa* = *Actinobacillus actinomycetemcomitans*; *Ec* = *Escherichia coli*; *Ea* = *Erwinia amylovora*; *Kp* = *Klebsiella pneumoniae*; nd = not determined; *Pa* = *Pseudomonas aeruginosa*; *Psa* = *Pseudomonas syringae* pv. *actinidiae*; *Pss* = *Pseudomonas syringae* pv. *syringae*; *Pto* = *Pseudomonas syringae* pv. *tomato*; *Se* = *Salmonella enterica* subsp. *enterica; Xap* = *Xanthomonas arboricola* pv. *pruni*; *Xav* = *Xanthomonas axonopodis* pv. *vesicatoria*; *Xf* = *Xylella fastidiosa*.

(Fmoc)/*tert*-butyl strategy. Fmoc-Rink-ChemMatrix (0.69 mmol/g), 3-(4-hydroxymethylphenoxy)propionic acid (PAC)-ChemMatrix (0.22 mmol/g), or Fmoc-Rink-4-methylbenzhydrylamine (MBHA) (0.71 mmol/g) resins were used as solid support. Fmoc-Rink-ChemMatrix and PAC-ChemMatrix resins were selected for the synthesis of peptides containing more than 14 residues. The PAC-ChemMatrix resin was employed to prepare C-terminal carboxylic acid peptides, whereas the Fmoc-Rink-ChemMatrix and the Fmoc-Rink-MBHA resins served for C-terminal peptide amides. Peptide elongation was carried out through sequential steps of Fmoc removal and coupling of the corresponding amino acid, as previously described (Caravaca-Fuentes et al. 2021; Oliveras et al. 2021). The Fmoc group was removed with piperidine/*N,N*-dimethylformamide (DMF). Couplings of the amino acids were carried out by treating the resin with the corresponding amino acid, *N,N*-diisopropylcarbodiimide and ethyl (hydroxyimino)cyanoacetate in DMF overnight. Once the peptide sequence was completed, each resulting peptidyl resin was treated with trifluoroacetic acid (TFA)/H_2O/triisopropylsilane (TIS) (95:2.5:2.5). Peptidyl resins that contained tryptophan and/or arginines were treated with TFA/H_2O/TIS/thioanisole/1.2-ethandithiol/phenol (81.5:5:1:5:2.5:5). Following TFA evaporation and diethyl ether extraction, the crude peptides were purified by reverse-phase column chromatography, lyophilized, analyzed by high-performance liquid chromatography (HPLC), and characterized by mass spectrometry. All peptides were obtained in excellent HPLC purities (≥94%), and their structure was confirmed by mass spectrometry (Supplementary Table S1).

Bacterial strains and growth conditions

All the experiments were carried out in officially authorized laboratories under Biosafety level 2+ containment conditions according to European and Mediterranean Plant Protection Organization (EPPO) (EPPO 2006) and the EU regulation (Commission Implementing Regulation [EU] 2020/1201 and 2021/2285) (EFSA Panel on Plant Health et al. 2018; European Union 2020, 2021). The *X. fastidiosa* strains used in this work were *X. fastidiosa* subsp. *fastidiosa* (*Xff*) TemeculaL, *Xff* IVIA 5387.2, *Xff* IVIA 5770, *X. fastidiosa* subsp. *pauca* (*Xfp*) DeDonno (DD1), *X. fastidiosa* subsp. *multiplex* (*Xfm*) IVIA 5901.2, and *Xfm* CFBP 8173 (Moll et al. 2021; Román-Écija et al. 2023). All strains were stored in Pierce's disease (PD) broth 2 (Davis et al. 1980) supplemented with glycerol (30%) and maintained at −80°C. When needed, strains were cultured in buffered charcoal yeast extract agar plates (Wells et al. 1981) except for motility experiments, in which case they were cultured in periwinkle wilt media (PW; Davis et al. 1981). Plates were kept at 28°C for 7 days. Afterward, colonies were scrapped and cultured in their corresponding media at 28°C for 7 additional days before being used in any of the experiments. When liquid cultures were required, PD2 or PD3 broth (Davis et al. 1981) was used. Cell suspensions were prepared in sterile succinate-citrate-phosphate buffer for bactericidal activity experiments, in sterile phosphate-buffered saline buffer for antibiofilm activity experiments, in PD2 or PD3 broth for microfluidic chamber and transmission electron microscopy (TEM) experiments, and in PD2 broth for plant experiments. For all experiments except for microfluidic chamber experiments, the suspensions were adjusted to an optical density at 600 nm (OD_{600}) of 0.32, which corresponds approximately to 10^8 CFU/ml, which was confirmed by plate counting in PD2 plates. For microfluidic chamber experiments, the suspensions were adjusted to an OD_{600} of 1.

Characterization of peptides

Bactericidal and antibiofilm activity and toxicity tests, such as tobacco leaf infiltration and hemolytic activity tests, were performed as previously described (Moll et al. 2021).

Bactericidal activity of the peptides against *Xff* IVIA5387.2 or *Xff* TemeculaL, depending on the experiment, was assessed by a contact test coupled with viable-quantitative PCR (v-qPCR) (Baró et al. 2020a; Moll et al. 2021). They were tested at a final concentration of 50 μM, using cecropin B (C1796, Merck, Spain) as a reference compound (Li and Gray 2003). Highly active peptides (reduction in viability >3 logs) were further tested at 12.5 and 3.1 μM to better characterize their bactericidal activity.

Antibiofilm activity was assessed as the ability to inhibit biofilm formation or the ability to disrupt mature biofilm using a crystal violet dye method (Moll et al. 2021; Raheem and Straus 2019). Peptides were tested at a final concentration of 50 μM against *Xff* IVIA 5387.2, except for those that exhibited a high bactericidal activity, which were tested at 3.1 μM to avoid the influence of their antibacterial activity in the biofilm formation. Peptide 1026 was included and tested at 50 μM as a reference compound (Moll et al. 2021). For biofilm disruption assays, the same protocol was carried out with a slight modification; peptides were added after 5 days of *Xff* IVIA 5387.2 incubation, and microplates were incubated at 28°C for 1 additional day under continuous shaking (120 rpm).

Peptides were evaluated at 50, 100, and 150 μM for their effect upon infiltration on tobacco leaves (*Nicotiana tabacum*) (Nadal et al. 2012), whereas hemolytic activity of peptides was tested at 150, 250, and 375 μM in erythrocyte suspensions of horse blood (Badosa et al. 2007).

Twitching motility on agar plates

Twitching motility was assessed on agar plates. Cells of each strain were scrapped from 7-day-old culture plates and were spotted with a plastic inoculation needle onto the surface of modified PW agar (no BSA, no red phenol and 1% agar) plates. Plates were incubated at 28°C for 4 days. The colony peripheral fringe morphology was observed each day with a Nikon Eclipse Ti inverted microscope (Nikon; Melville, NY, U.S.A.) using phase contrast and a Nikon DS-Qi digital camera (Nikon) controlled by NIS-Elements Advanced Research 3.01 (Nikon). Four fringe-width measures per colony in six colonies per strain were carried out using the ImageJ software (version 1.8.0_112; National Institutes of Health [NIH], U.S.A.). Three independent experiments were conducted.

To assess the effect of peptides on twitching motility of *Xff* TemeculaL, the peptides were solubilized in sterile Milli-Q water to a stock concentration of 1 mM, filter-sterilized through a 0.22-μm pore-sized filter, and included in the modified PW agar plates (same as above) to a final concentration of 3.1, 12.5, 25, and 50 μM. Sterile Milli-Q water was used as not treated control (NTC). BSA (15260-037, Gibco, NY, U.S.A.) at 6 g/liter was included as positive control because it inhibits the motility of *X. fastidiosa* (Galvani et al. 2007). Cells were scrapped, spotted on modified PW agar plates, and incubated at 28°C for 4 days. Next, the colony peripheral fringe width was measured as explained above. Initial observations were performed at 12.5 μM to minimize the interference of other activities on the effect on motility. The ratio of the twitching fringe width was calculated according to the formula *Ft/Fc*, where *Ft* and *Fc* are the average fringe width of the treatment and NTC, respectively. Two independent experiments were performed. Median effective concentration (EC_{50}) of the peptides was calculated with the EC_{50} calculator of ATT Bioquest using the two-parameter model (AAT Bioquest 2024).

Twitching motility in microfluidic chambers

The microfluidic chamber was constructed as previously described (Chen and De La Fuente 2020; De La Fuente et al. 2007b). Briefly, the microfluidic chip consists of a molded polydimethylsiloxane body with two parallel microchannels (80 μm wide, 50 μm deep, and 3.7 cm long) on a surface sealed by a cover glass. Each microchannel had two inlets and one outlet connected to a 20-cm tubing with a syringe adaptor at the end. Depending on the experiment, PD2 or PD3 broth was used, and broth, a bacterial suspension in broth, or the peptide mixed with broth were pumped into the microfluidic chamber through the inlets. To compare the twitching motility of *Xff* TemeculaL and *Xff* IVIA 5387.2, PD2 broth was introduced into the chamber through the upper inlets, whereas the bacteria cells of both strains were introduced through the side inlets (Supplementary Fig. S1A). To determine the effect of the peptides on the twitching motility, cells of *Xff* TemeculaL were introduced through the top inlets, whereas PD3 broth (NTC) or the peptide mixed with PD3 broth (treatment) were introduced through the side inlets (Supplementary Fig. S1B). The peptides tested were BP100 and FV7, which were

filter-sterilized and diluted in PD3 broth to a final concentration of 3.1 μM. Bacterial suspensions of *Xff* TemeculaL or *Xff* IVIA 5387.2 were prepared as described in the growth conditions section and were used to fill two 1-ml plastic syringes (Becton Dickinson & Company, Franklin Lakes, NJ, U.S.A.). The PD3 broth, with or without peptides, was used to fill 5 ml plastic syringes (Becton Dickinson and Company, Franklin Lakes, NJ, U.S.A.). The syringes were connected to the tubbing, and the flow was controlled by automated syringe pumps (Pico Plus; Harvard Apparatus, Holliston, MA, U.S.A.) (Supplementary Fig. S1C). Microfluidic chambers and connecting tubing were flushed and filled with the liquid media prior to the introduction of the bacterial cell suspension. Cell suspensions were initially introduced in both channels at 10 μl/min for 25 min. Afterward, the flow was reduced to 0.3 μl/min for 35 min to allow cell adhesion to the cover glass surface. Finally, the inlet for the cell suspension was clamped, and only PD3 broth (with or without peptide) was allowed into the chamber. The microfluidic chamber was monitored with a Nikon Eclipse Ti inverted microscope (Nikon, Melville, NY, U.S.A.) using Nomarski differential interference contrast optics and phase contrast. Time-lapse images were acquired every 30 s using a Nikon DS-Qi digital camera (Nikon) controlled by NIS-Elements Advanced Research 3.01 (Nikon) for 60 h. To assess the twitching motility, six cells per treatment were selected randomly, and their twitching distance was measured using the NIS-Elements Advanced Research 3.01 (Nikon) software for 12-h intervals. All experiments were conducted at room temperature (25°C), and each experiment was repeated 3 times. To analyze the results, the flow rate and the length and dimension of the tubing were taken into account to let the peptide to come into contact with the cells found in the microfluidic channels where the observation was made, which requires approximately 24 h.

To confirm that BP100 had minimal effect on the culturability or viability of *Xff* TemeculaL, two different tests were carried out. The first one consisted of collecting the cells from the microfluidic chamber once the experiment was finalized. Next, serial dilutions in PD3 media were performed, plated on PD3 plates, incubated for 7 days at 28°C and, afterward, CFU per milliliter were determined. The second one consisted of testing the bactericidal activity of BP100 against *Xff* TemeculaL at different concentrations using the method explained above.

Transmission electron microscopy

The presence of type IV pili in *Xff* TemeculaL cells was assessed by TEM after the treatment with BP100 in solid and liquid media. Regarding the solid media, the cells were spotted on modified PW agar plates with BP100 at 12.5 μM or sterile Milli-Q water as NTC, and plates were incubated at 28°C for 4 days as described above. Next, bacterial cells from the peripheral fringe were collected by scraping and were resuspended in 200 μl of sterile distilled water. Regarding the liquid samples, a suspension of 10^7 cells per milliliter in PD3 was incubated for 24 h at 28°C under continuous shaking (120 rpm). Afterward, 4.5 ml of cell suspension was transferred into two sterile 50-ml centrifuge tubes. In one of the tubes, 0.5 ml of BP100 was added to a final concentration of 3.1 μM, and in the NTC, water was used instead. The tubes were incubated for 24 h at 28°C under continuous shacking (120 rpm).

In both cases, afterward, 10 μl of planktonic cells was recovered from each tube and were deposited on 300-mesh carbon-coated copper grids (Electron Microsocpy Sciences, Hatfield, PA, U.S.A.), and they were allowed to settle for 10 min. After that, the grid was negatively stained with 20 μl of uranyl acetate two times for 1 min and subsequently washed two times with Milli-Q water for 1 min. Finally, they were observed with a TEM JEM-1400 (JEOL, Tokyo, Japan). The percentage of cells with type IV pili and the length of pili were determined for each treatment using the ImageJ software (version 1.8.0_112, NIH, U.S.A.). A minimum of 30 cells were analyzed per treatment.

Plants and greenhouse conditions

One-year-old almond plants (*Prunus dulcis*) from cv. Avijor (provided by Agromillora, Spain) were used for the experiments. All plants were maintained in 0.8-liter pots (sphagnum peat with wood fiber [10%], calcium carbonate [9 g/liter], nitrogen-phosphorus-potassium (NPK) fertilizer [1 kg/m^3] and microelements) in an environmentally controlled quarantine greenhouse. The photoperiod consisted of 16 h of light at 25 ± 2°C (day) and 8 h of darkness at 18 ± 2°C (night). Before and during the experiments, plants were watered to saturation every 3 days and fertilized with a 200-ppm solution of NPK (20:10:20) once a week. In addition, throughout the experiments, standard treatments with insecticide and acaricide were performed to avoid presence of insect vectors or pests. Infected plants were cultivated in a Biosafety level 2+ quarantine greenhouse authorized by the Plant Health Services according to EPPO recommended containment conditions (EPPO 2006) and were maintained taking into account the consideration of *X. fastidiosa* as a quarantine pathogen in the EU (European Union 2019, 2021).

Effect of peptides on population levels of *X. fastidiosa*, ALS severity, and leaf physiological parameters in almond plants

The effect of BP100 on population levels of *Xff* IVIA 5387.2, ALS severity, and on leaf physiological parameters in inoculated almond plants of cv. Avijor was assessed. The treatment with the peptides BP178 with bactericidal and defense elicitor activity and KSLW-FV7 with bactericidal activity were included as references for comparison purposes.

Peptides were applied 1 day before *Xff* inoculation and 3 and 7 days postinoculation (dpi) through endotherapy, and each application consisted of three injections of 10 μl at 20 mM, as described previously (Supplementary Fig. S2) (Moll et al. 2022). Not-treated plants (NTC) were included using water instead of the peptides. The inoculation of *Xff* was performed with three injections of 10 μl of a suspension of *Xff* at 10^8 CFU/ml, as described in Baró et al. (2021) (Supplementary Fig. S2). Not-inoculated controls were included by injecting water instead of the bacterial suspension.

X. fastidiosa population levels were assessed at 15, 40, 65, and 90 dpi for all the treatments (not-inoculated, NTC, BP178, KSLW-FV7, and BP100). The experimental design consisted of three replicates of three plants per each treatment and sampling time (15, 40, 65, and 90 dpi) (180 plants). A second experiment was carried out by only sampling at 40 dpi (45 plants). Samples were collected, and the levels of viable cells in sap were analyzed by v-qPCR, as described in Baró et al. (2021).

In another set of experiments, ALS symptoms on treated plants were assessed at 0, 15, 30, 47, 58, 70, 82, and 90 dpi, following the severity scale previously described (Baró et al. 2021). The experimental design consisted of three replicates of three plants per each treatment (not-inoculated, NTC, BP178, KSLW-FV7, and BP100) (45 plants). Two independent experiments were performed. Additionally, chlorophyll, flavonol, and anthocyanins content were determined by leaf transmittance, providing an index that is proportional to the content of each compound within the leaf using the DUALEX sensor (METOS Iberia, Seville, Spain) at the same timestamps (Camino et al. 2021; Cerovic et al. 2012). A not-inoculated control was also included because it has been described that *X. fastidiosa* infection alters the previously mentioned parameters (Camino et al. 2021; Pereira et al. 2019; Zarco-Tejada et al. 2018). Briefly, measurements were taken on four leaves above the highest point of inoculation between the center and the margin of the leaves. A total of 12 leaves were pooled from three different plants for each replicate.

Analysis of xylem vessels by scanning electron microscopy (SEM) in BP100-treated almond plants infected with *X. fastidiosa*

The effect of BP100 treatment on the xylem vessels of infected almond plants was analyzed through SEM. Almond plants were treated with BP100 and inoculated with *Xff* IVIA 5387.2 as described above. Not-treated plants (NTC) inoculated with *Xff* and not-inoculated plants were included as references. Three disks of 1- to 2-mm thickness stem cross-sections were gathered from 4 cm above the highest peptide treatment point found in upward 1 at 90 dpi (Supplementary Fig. S2). A total of three replicates were obtained from three different plants of each treatment. Samples were chemically fixed with glutaraldehyde EM Grade (2.5%) and paraformaldehyde

(4%) in a sodium cacodylate buffer solution (0.1 M) for 4 h at 4°C, followed by a solution of OsO_4 (1%) in a sodium cacodylate buffer solution for 1.5 h at room temperature. Samples were rinsed twice with the sodium cacodylate buffer solution and were dehydrated in an ethanol solution series of 50, 75, 90, and 100% for 10 min. The last step was repeated 3 times. Samples were critical point–dried (EMITECH K850, Quorum Technologies, Laughton, U.K.), mounted on carbon stubs, and sputter coated with carbon (EMITECH K950 Turbo, Quorum Technologies, Laughton, U.K.). Coated sections were examined under a field emission SEM (CLARA, TESCAN, Brno, Czech Republic) at an accelerating voltage of 5 keV. Treated plants xylem vessels were compared with not-inoculated and NTC plant vessels. Frequency of vessels with biofilm or biofilm associated with tyloses (Supplementary Fig. S3) was determined for the three disks of the three replicates.

Data analysis

The significance of the effect of the peptides on antibacterial activity, antibiofilm activity, leaf infiltration effect, hemolytic activity, and twitching motility was determined with a one-way analysis of variance (ANOVA). To test the significance of the effect of peptides on *Xff* population levels, ALS symptoms and leaf physiological parameters (chlorophyll, flavonol, and anthocyanin contents) over time, a repeated measures ANOVA was used. To test the significance of the effect of peptides and the experiments on ALS symptoms a two-way ANOVA was used. In all cases, means were separated according to the Duncan's test at a $P < 0.05$ (IBM SPSS Statistics for Windows, Version 25.0, released in 2017 by IBM Corp, Armonk, New York, U.S.A.). Correlation between ALS symptoms and leaf physiological parameters was assessed using Pearson's correlation with the same program indicated above.

Results

Twitching motility of *X. fastidiosa* strains

The twitching motility of six *X. fastidiosa* strains (*Xff* TemeculaL, *Xff* IVIA 5387.2, *Xff* IVIA 5770, *Xfm* IVIA 5901.2, *Xfm* CFBP 8173, and *Xfp* DD1) was assessed in agar plates (Fig. 1A). Only *Xff* TemeculaL exhibited the presence of a peripheral colony fringe, which increased over time and is indicative of twitching motility. Regarding *Xfp* DD1, some microcolonies can be observed outside the periphery that were probably dispersed during handling. The fringe width of *Xff* TemeculaL was measured each day (Fig. 1B). A lag phase was observed during the first day, followed by a linear increase of the fringe width up to the fourth day, with a maximum movement rate of 102 μm/day on agar.

The twitching motility of *Xff* TemeculaL and *Xff* IVIA 5387.2 was also assessed in microfluidic chambers (Fig. 1C). In particular, *Xff* TemeculaL moved at a rate of 0.84 μm/min (1210 μm/day), which was almost 12-fold faster than on agar. Interestingly, *Xff* IVIA 5387.2 showed twitching motility at a rate of 0.29 μm/min, almost threefold slower than TemeculaL.

Biological activities of the selected peptides

Bactericidal activity. The 17 selected peptides were tested for bactericidal activity against *Xff* IVIA 5387.2, and cecropin B was included as a reference (Fig. 2). Peptides were classified into statistically different groups ($P < 0.05$; Supplementary Table S2). KSLW-FV7, 1036, BP534, BP535, BP536, and RIJK2 displayed very high activity, with a log reduction of cell viability >3.5. BP100, FV7-BP100, BP100-FV7, FV7-BP16, BP16-FV7, and FV7-KSLW showed moderate activity, with a 1 to 2 log reduction of cell viability. The remaining peptides exhibited low or very low activity, with <0.5 log reduction of cell viability.

Peptides that showed very high bactericidal activity against *X. fastidiosa* were further tested at 12.5 and 3.1 μM (Supplementary Table S2). KSLW-FV7 was the most active peptide, with a 4 and 3.3 log reduction at 12.5 and 3.1 μM, respectively, being more active than the reference peptide cecropin B. Peptides 1036, BP534, and BP535 showed log reductions of cell viability ranging from 3.1 to 4.0 at 12.5 μM and between 1.5 and 1.9 at 3.1 μM. The activity of BP536 and RIJK2 decreased at 12.5 μM, exhibiting a 2.4 and 1.8 log reduction, respectively.

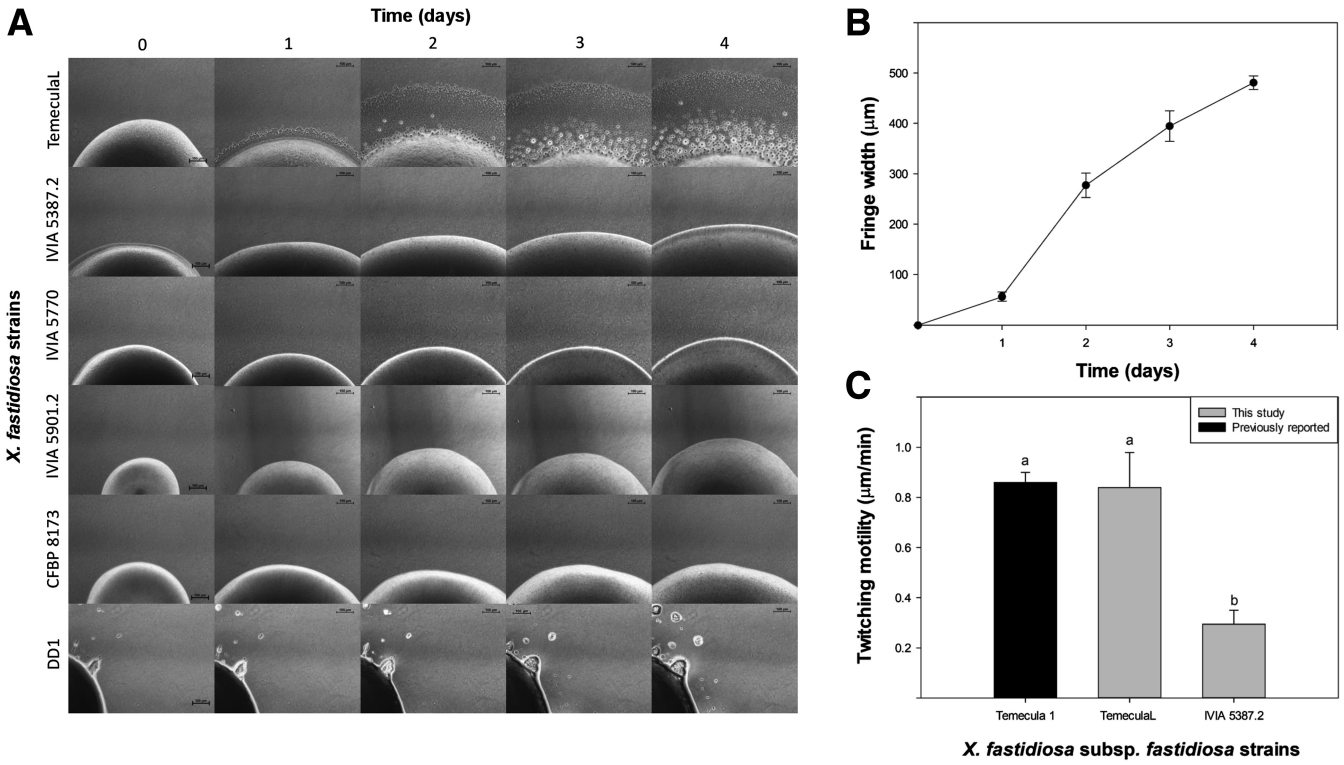

Fig. 1. Twitching motility of not-treated *X. fastidiosa* strains. **A,** *X. fastidiosa* colonies with peripheral fringes on modified periwinkle wilt media (PW) agar plates. The black bar represents 100 μm. **B,** Colony fringe width of *X. fastidiosa* subsp. *fastidiosa* TemeculaL on modified PW agar plates throughout 4 days. Values are the means of six replicates, and error bars represent the confidence interval ($\alpha = 0.05$). **C,** Twitching speed of *X. fastidiosa* strains under microfluidic chamber conditions. Values are the means of six replicates, and error bars represent the confidence interval ($\alpha = 0.05$). Temecula 1 values were obtained from the literature (De La Fuente et al. 2007a).

Antibiofilm activity. The 17 selected sequences were tested for their antibiofilm activity against *Xff* IVIA 5387.2 (Fig. 2; Supplementary Table S2). To minimize the influence of their antibacterial activity in biofilm formation, peptides with very high antibacterial activity were tested at 3.1 μM. Peptide 1026 was included as a reference control (ratio of biofilm formation 0.01). Peptides were classified into statistically different groups depending on their ability to inhibit biofilm formation ($P < 0.05$). Except for BP100 and BP16, the other 15 peptides exhibited high biofilm formation inhibition (ratios ranging from 0.04 to 0.24). It is interesting to note that KSLW-FV7, 1036, BP534, BP535, BP536, and

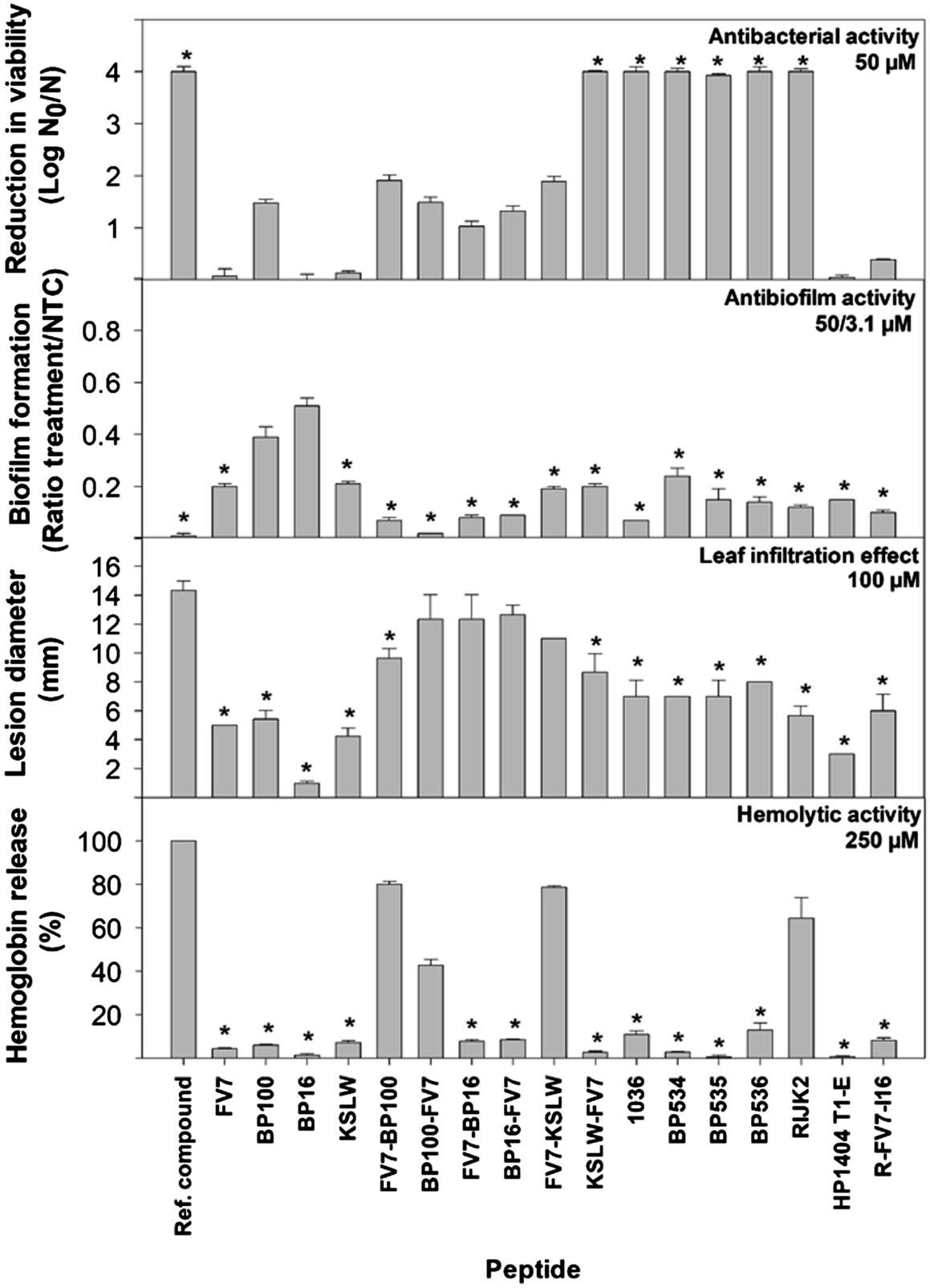

Fig. 2. Bactericidal and antibiofilm activity against *X. fastidiosa* subsp. *fastidiosa* IVIA 5387.2, tobacco leaf infiltration effect, and hemolytic activity of peptides. Values are the means of three replicates, and error bars represent the confidence interval ($\alpha = 0.05$). The asterisk (*) indicates the peptides that have the best values for each activity according to the Duncan's test ($P < 0.05$). The reference (Ref.) compounds used were cecropin B for bactericidal activity, 1026 for antibiofilm activity, and melittin for tobacco leaf infiltration effect and hemolytic activity. For antibiofilm activity, peptides with very high bactericidal activity were diluted at 3.1 μM (KSLW-FV7, 1036, BP534, BP535, BP536, and RIJK2).

RIJK2, with very high antibacterial activity, also displayed high anti-biofilm activity at 3.1 μM.

The ability of peptides to disrupt mature biofilm was tested at 50 μM against a 5-day-old biofilm of *Xff* IVIA 5387.2 (Supplementary Table S2). Peptides were classified in two statistically different groups ($P < 0.05$). Only a moderate activity was observed for BP100-FV7, FV7-KSLW, RIJK2, and HP1404 T1-E, with a ratio of biofilm disruption between 0.65 and 0.78.

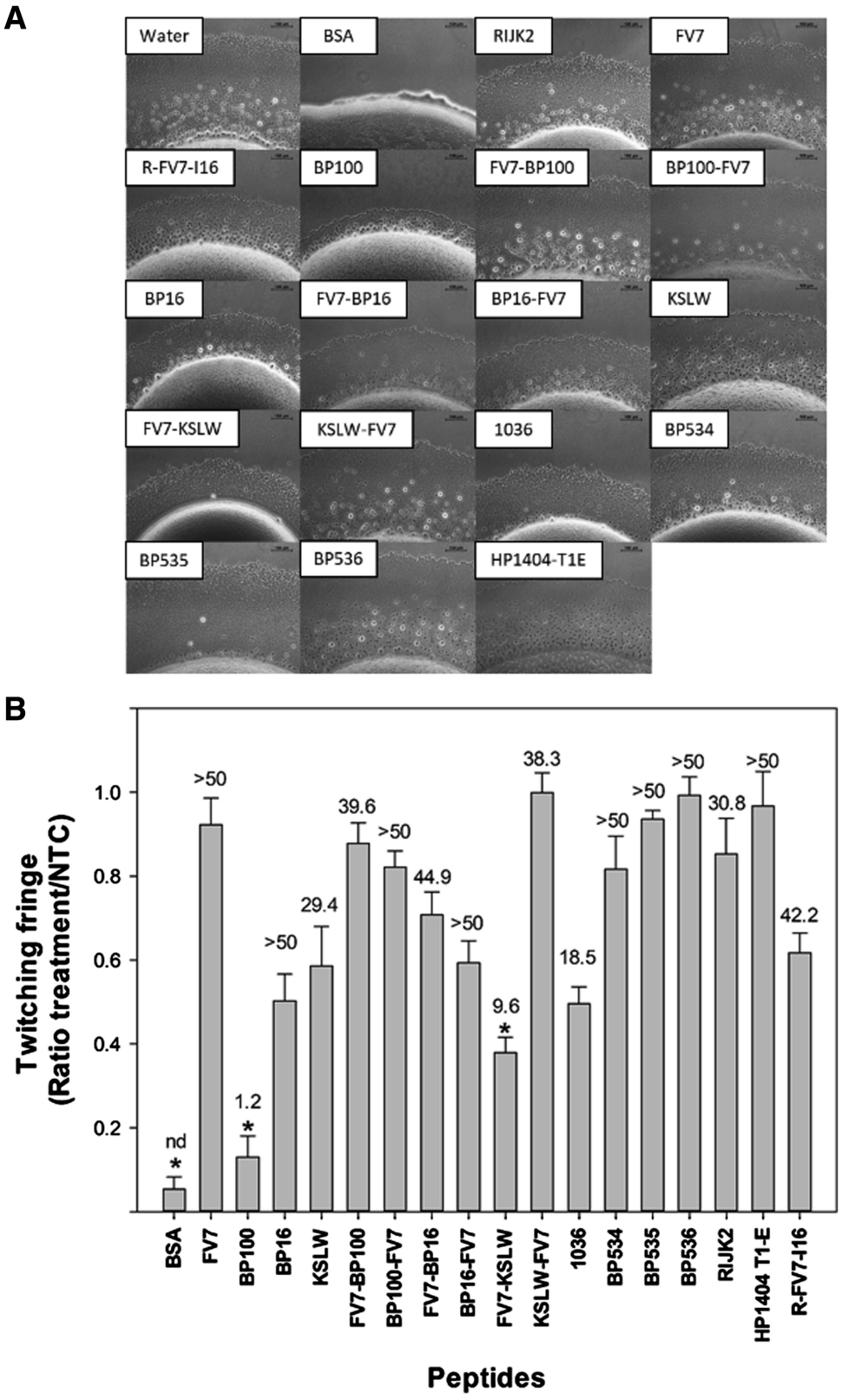

Fig. 3. Peptide effect on *X. fastidiosa* subsp. *fastidiosa* TemeculaL twitching motility on modified periwinkle wilt media (PW) agar plates. **A,** *X. fastidiosa* subsp. *fastidiosa* TemeculaL colonies with peripheral fringes on modified PW agar plates. The black bar on the images represents 100 μm. **B,** Colony fringe-width ratio of *X. fastidiosa* subsp. *fastidiosa* TemeculaL. Values of the graph bars are the means of six replicates, and error bars represent the confidence interval ($\alpha = 0.05$). The asterisk (*) indicates the peptides with the lowest ratio of twitching fringe according to the Duncan's test ($P < 0.05$). The numeric values on top of the graph bars indicate the median effective concentration (EC_{50}) calculated for each peptide. BSA = bovine serum albumin; nd = not determined.

Effect of peptides on tobacco leaves and hemolytic activity. The effect of peptides on eukaryotic cells was assessed on tobacco leaves and erythrocytes. The 17 selected peptides and the reference peptide melittin were infiltrated into the mesophyll of tobacco plant leaves at 50, 100, and 150 μM (Supplementary Table S3). Lesion diameter at 100 μM is shown in Figure 2. The reference peptide melittin was the one that caused the greatest lesion (14.3 mm). All tested peptides caused a lesion ranging from 1 to 9.7 mm, which was significantly lower than the reference compound, except for BP100-FV7, FV7-BP16, BP16, and FV7-KSLW, which presented values closer to melittin ranging from 11 to 12.7 mm. Hemolytic activity of the peptides was determined on horse blood erythrocytes at 150, 250, and 375 μM and compared with the reference peptide melittin (Supplementary Table S3). Percentage hemolysis at 250 μM is shown in Figure 2. Except for four sequences, the other peptides were low-hemolytic (≤13% hemolysis at 250 μM). In all cases, it was significantly different than melittin ($P < 0.05$).

Effect of peptides on the motility of *X. fastidiosa*

The influence of the 17 selected peptides on the motility of *Xff* TemeculaL was determined by evaluating the changes on the morphology and the width of the colony fringe of the bacteria after being in contact with the peptides at 12.5 μM for 3 days (Fig. 3). Initial observations were performed at 12.5 μM to minimize the interference of other activities on the effect on motility. BSA was included as a reference. Peptides were classified in statistically different groups based on their effect on colony fringe reduction (Supplementary Table S2). BP100 was the most active peptide, reducing the twitching fringe by 87% (ratio of twitching fringe of 0.13) with no significant differences ($P < 0.05$) with BSA (0.13 versus 0.05; twitching motility reduction of 87 versus 95%). FV7-KSLW also caused an important reduction of the motility of *Xff* (twitching fringe ratio of 0.38; 62% of twitching motility reduction). BP16, KSLW, FV7-BP16, BP16-FV7, 1036, and R-FV7-I16 exhibited a moderate reduction of the motility of *Xff* Temecula, with twitching fringe ratios ranging from 0.50 to 0.72. Twitching fringe ratios >0.82 were observed for the other sequences. In addition, the EC_{50} was calculated for all peptides, BP100 and FV7-KSLW being the ones with the lowest value (1.2 and 9.6 μM, respectively).

The effect of BP100 on twitching motility at 3.1 μM was confirmed under microfluidic chamber conditions and compared with that of FV7 as an NTC (Fig. 4). Throughout the experiment, the NTC showed a constant average twitching motility rate of 0.25 μm/min. Treatment with BP100 caused a sevenfold decrease in twitching motility at the end of the experiment ($P < 0.01$). In contrast, as expected, FV7 did not display significant differences in twitching motility rate compared with the NTC ($P = 0.56$). No significant differences were found between the three independent experiments performed ($P > 0.05$). BP100, at 3.1 μM, did not have bactericidal activity against *Xff* TemeculaL because cells recovered from BP100 channels from the microfluidic chamber maintained culturability (Supplementary Fig. S4A) and showed almost no viability reduction in a contact test (Supplementary Fig. S4B).

Effect of BP100 on type IV pili in TemeculaL cells

The presence of type IV pili in *Xff* TemeculaL cells was assessed by TEM in the NTC and after the treatment with BP100. In both samples, cells showed type IV pili, and no morphological differences were observed (Fig. 5). Type IV pili were present in 39 ± 3% of cells treated with BP100 and in 45 ± 3% in the NTC. The average type IV pili length was of 4.78 ± 0.35 μm in cells treated with BP100 and of 4.61 ± 0.51 μm in the NTC. Interestingly, no significant differences were found between treatments regarding the frequency ($P = 0.07$) and the length ($P = 0.23$) of type IV pili.

Colonization of *X. fastidiosa* in treated almond plants

Viable *Xff* cell populations in almond plants were determined after treatment with BP100 and compared with those of plants treated with BP178 and KSLW-FV7 and an NTC. No significant differences were observed between the results obtained from the two independent experiments at 40 dpi ($P = 0.32$). The population levels of *X. fastidiosa* at 15, 40, 65, and 90 dpi are shown in Fig. 6. In all treatments, there was a first stage (15 to 40 dpi) that showed an exponential growth of *X. fastidiosa* until a maximum was reached between 40 and 65 dpi, depending on the zone of the plant analyzed. In a second stage (65 to 90 dpi), the viable cells of *X. fastidiosa* in sap decreased. All treatments showed overall significant differences through a repeated measures ANOVA in all the plant sections that were analyzed (downward and upward zones 1 and 2) when compared with the NTC ($P < 0.05$). BP100 caused a significant reduction in viable *Xff* cells in sap compared with the NTC in almost all plant parts analyzed, with a decrease between 1 and 2 log. The effect of BP100 on the *Xff*-viable population did not differ from that of the BP178 and KSLW-FV7, except in the upward zones, were BP178 caused a greater reduction of viable cells in sap.

ALS symptoms development and leaf physiological parameters progression in treated almond plants

The effect of the peptide BP100 on disease severity and leaf physiological parameters (chlorophyll, flavonol, and anthocyanin content) was determined over a period of 90 dpi (Fig. 7; Supplementary Figs. S5 and S6) and compared with the treatments with BP178 and KSLW-FV7 and an NTC. The NTC plants were the most affected during the whole experiment, and most of them started to show marginal necrosis in almost half of the leaves at 90 dpi. ALS symptoms started between 30 and 47 dpi, and disease severity increased over time. Symptoms were reduced in plants treated with BP100, BP178, and KSLW-FV7, and significant differences were observed compared with the NTC plants throughout the two experiments. The disease

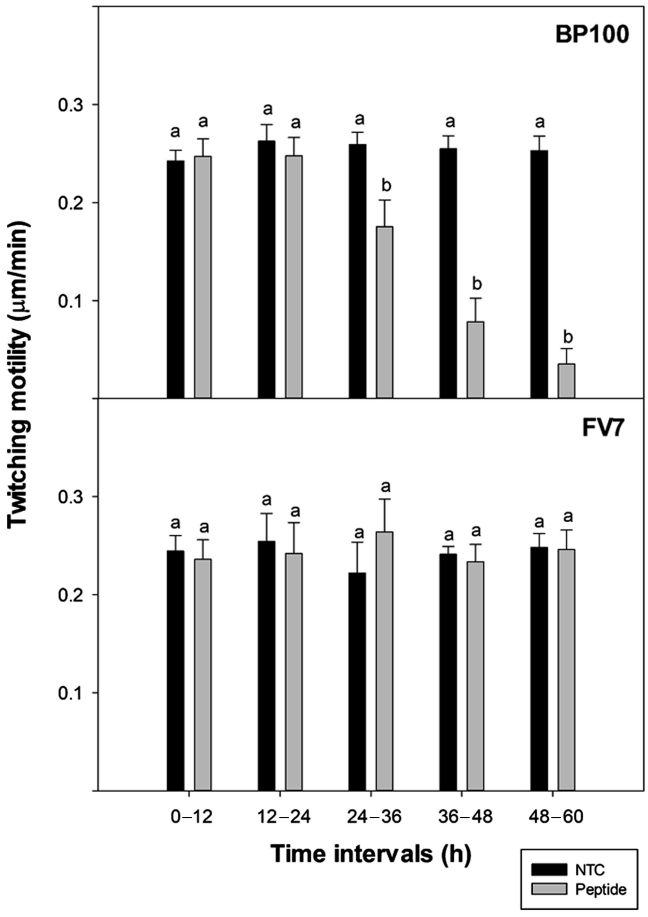

Fig. 4. Peptide activity on *X. fastidiosa* subsp. *fastidiosa* TemeculaL twitching motility under microfluidic chamber conditions for the channel treated with the peptide at 3.1 μM (BP100 or FV7) and the not-treated control (NTC) channel. Values are the means of average twitching speed of six replicates for 12-h intervals, and error bars represent the confidence interval ($\alpha = 0.05$). The letters correspond to the means comparison between the treatment and the NTC at each 12-h time interval. Means sharing the same letters within the same time interval are not significantly different ($P < 0.05$) according to the Duncan's test.

severity reduction for the plants treated with BP100, BP178, and KSLW-FV7, compared with the NTC at 82 dpi in the first experiment was of 71, 58, and 50%, respectively (Fig. 7), and of 86, 69, and 67% reduction in the second experiment (Supplementary Fig. S6). In addition, significant differences were found between BP100, BP178, and KSLW-FV7 in both experiments, BP100 being the one that caused the highest disease severity reduction.

The NTC showed differences regarding the leaf physiological parameters when compared with the not-inoculated control defining the maximum and minimum values for each parameter. Specifically, the not-inoculated control presented the best performance when compared with the NTC (higher chlorophyll and lower flavonol and anthocyanin content). The treatments showed an intermediate effect, being more similar to the not-inoculated control. In general, the leaf physiological parameters progression of inoculated plants can be divided in two phases, the first one being from 0 to 47 dpi and the second one from 47 to 90 dpi. During the first phase, the values of the parameters for the NTC and treated plants were similar to the not-inoculated plants, which correlated with low disease symptoms. Interestingly, during this phase, the flavonol content for BP100-treated plants was even lower than the one found in the not-inoculated plants until 70 dpi. In the second phase, a reduction in chlorophyll levels and an increase in flavonol and anthocyanin levels was observed in NTC plants compared with not-inoculated plants, which is consistent with the increase in disease symptoms. Treatment with BP100 caused an increase in chlorophyll (2.2-fold) and reduction of flavonol and anthocyanin content (54 and 56%, respectively) at 82 dpi when compared with the NTC.

Interestingly, a high correlation between data from disease severity and leaf physiological parameters was found. Specifically, as assessed by Pearson's correlation test, a coefficient value of –0.93 was obtained for chlorophyll content, 0.90 for flavonol content, and 0.84 for anthocyanin content ($P < 0.01$).

Effect of the treatments in the structure of the xylem vessels of infected almond plants

The effect of BP100 on the xylem vessels of infected almond plants was assessed at 90 dpi. As expected, the xylem vessels of the plants treated with BP100 showed differences when compared with the not-inoculated control and the NTC (Fig. 8). The not-inoculated plants did not show biofilm-like structures but exhibited a few small tyloses attached to the walls in 4 ± 1.2% of xylem vessels. Most of the xylem vessels found in the inoculated plants (NTC) showed biofilm-like structures (87.1 ± 1.4%), presence of tyloses, or a combination of both and also showed vessels that were partially or completely occluded (Supplementary Fig. S3). Xylem vessels of plants treated with BP100 were similar to the not-inoculated plants and showed only a 34.3 ± 1.3% of xylem vessels affected with biofilm-like structures.

Discussion

Interference of motility using chemical compounds can be a strategy for disease control, but the number of compounds that have been reported to interfere with this process is limited and not widely studied (Chatterjee et al. 2008c; Roper et al. 2019). Twitching motility of *X. fastidiosa* is a key process involved in the disease development in infected hosts (Pereira et al. 2019; Shi and Lin 2016). In the present work, we identified new peptides that inhibit the motility of *X. fastidiosa* and protect almond plants against ALS.

We have found that only *Xff* TemeculaL showed the colony fringe characteristic of twitching motility. Although, in the images of *Xfp* DD1 colonies outside the main colony margin can be observed, these are probably the result of the handling process because this strain is stickier than their counterparts. Our observations are in accordance

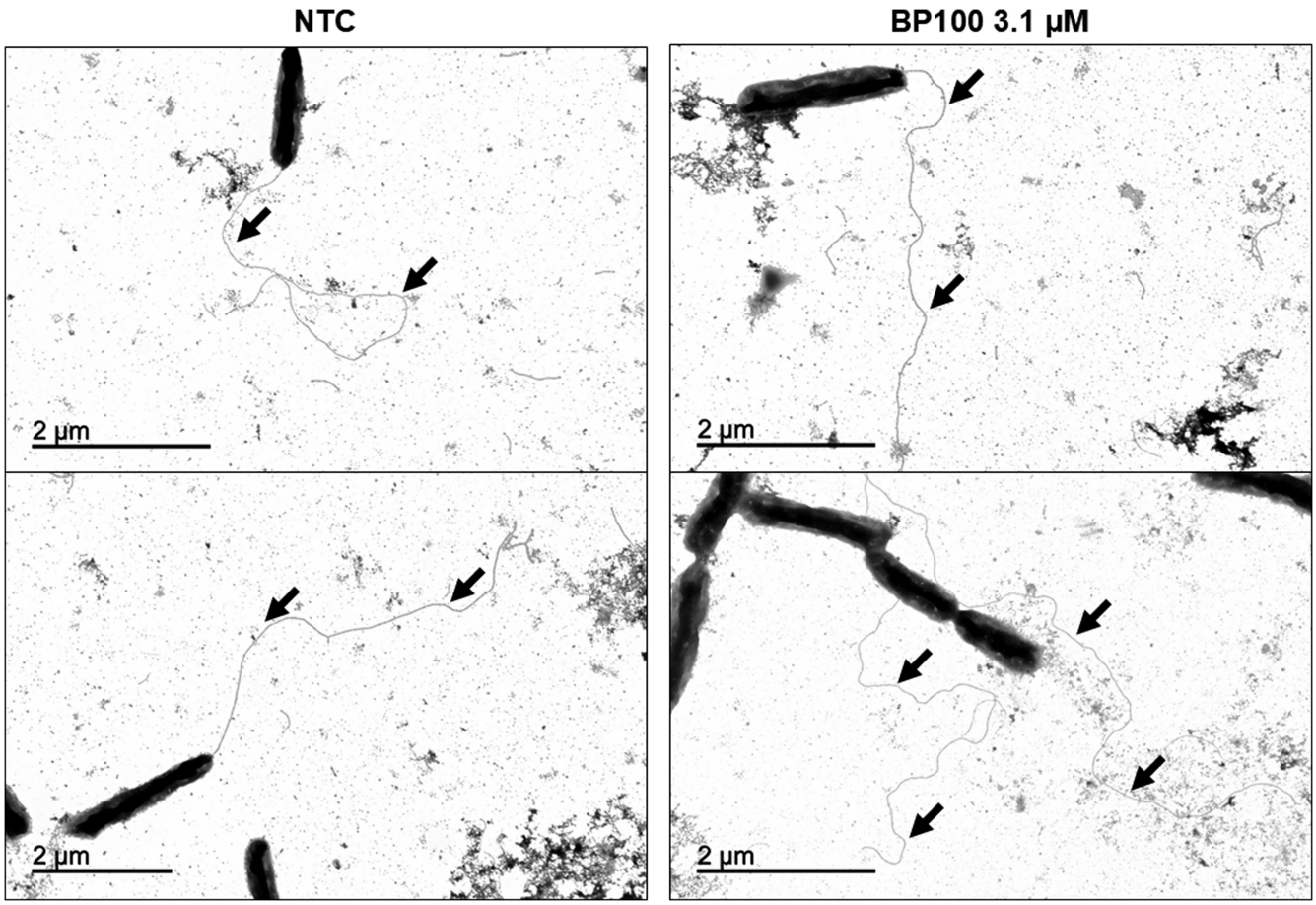

Fig. 5. Transmission electron micrographs of negatively stained cells of *Xylella fastidiosa* subsp. *fastidiosa* TemeculaL. Black arrows indicate type IV pili, which are generally found at one of the poles of the cells. The black bar represents 2 μm.

with previous reports in which the strain *Xff* TemeculaL presented fringe, whereas *Xfm* 5901.2 and *Xfp* DD1 have been reported to not showcase one (D'Attoma et al. 2020; Merfa et al. 2023; Román-Écija et al. 2023). Interestingly, the strain *Xff* IVIA 5387.2 showed twitching motility in microfluidic chambers in spite of the lack of a colony fringe when spotted on plates. However, its twitching motility rate was threefold lower than in *Xff* TemeculaL. The lack of fringe on agar could be caused by motility of *Xff* IVIA 5387.2 that may be dependent on external stimulus such as a pull owing to the flow of media or sap that only happens under microfluidic conditions or in planta (Meng et al. 2005). Another explanation would be that, because twitching motility on agar is slower than in liquid media and *Xff* IVIA 5387.2 presents a lower twitching motility speed in liquid compared with TemeculaL, the cell multiplication and expansion of the colony could be faster than its motility on agar, obscuring the fringe, as it was observed in the case of *X. fastidiosa* SC 17A97 (Galvani et al. 2007). This highlights the need to confirm the twitching motility of *X. fastidiosa* using several methods because one would not be sufficient. Based on these observations, TemeculaL was selected to be used in all of the in vitro motility-related experiments of this work.

The inhibitory effect of peptides on motility can be influenced (or masked) by other activities, such as bactericidal or antibiofilm activities. To minimize the influence of these activities, they were determined for each peptide. Interestingly, KSLW and FV7 had very low bactericidal activity, but its conjugation resulted in peptides with higher activity. Remarkably, the peptide conjugate KSLW-FV7 displayed higher bactericidal activity than its counterpart FV7-KSLW, indicating that the order of their conjugation has an important influence in the activity of the conjugates, as reported in previous studies (Caravaca-Fuentes et al. 2021; Horn and Neundorf 2018; Oliveras et al. 2022). Regarding the bactericidal and antibiofilm activity of the sequences derived from 1036, no significant differences were found between them, which indicates that these activities are not affected by the modifications incorporated in the sequence. In the present work, as well in a previous one (Moll et al. 2021), peptides exhibited a dose-effect relationship for bactericidal and antibiofilm activity. Therefore, at given concentrations, such as those <12.5 μM, these activities would be expected to have minimal interference in the twitching motility experiments.

To the best of our knowledge, this is the first report on peptides that influence the twitching motility of *X. fastidiosa*. The most active peptide identified was BP100, which reduced cells' motility on agar plates and under microfluidic chamber conditions. The peptide had no bactericidal activity against *Xff* cells at the used concentrations and, interestingly, did not affect type IV pili presence and morphology. These results could indicate that the peptide does not affect the synthesis of the type IV pili, but it may disrupt its functionality. The mechanism of action of BP100 on twitching motility has not been elucidated yet, but a hypothesis would be that it could interact with an extracellular component altering their functionality, such as the adhesins (*pilY*1-1-3) or the minor pilins (*pilEVWX1-2* and *fimT1-3*) of the type IV pili, which have been described to be key for motility (Merfa et al. 2023). BP100 could also interact with intercellular components of the type IV pili because it has been described as a cell-penetrating peptide in plant and mammalian models (Eggenberger et al. 2011; Yilmaz et al. 2021). Nevertheless, no studies regarding the cell-penetrating capabilities of BP100 have been carried out in gram-negative bacteria, but how it interacts with their plasmatic membrane has been described (Riesco-Llach et al. 2024). The peptide could interact with intracellular targets inhibiting enzymes related to the biosynthesis of DNA or RNA and have an effect on the

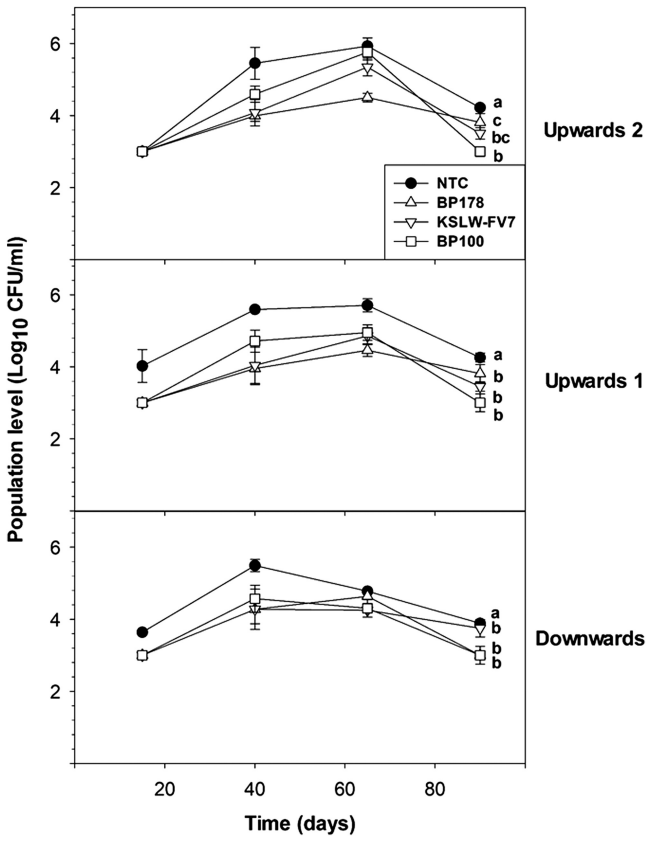

Fig. 6. Effect of the treatments (BP178, KSLW-FV7, BP100) on *X. fastidiosa* population levels in the sap of almond plants at 15, 40, 65, and 90 days postinoculation in the three sections that were sampled (downward, upward 1, and upward 2). Values are the means of three biological replicates of three plants each, and error bars represent the confidence interval (α = 0.05). Different letters between treatments indicate significant overall differences between the treatments for each analyzed section according to Duncan's test ($P < 0.05$).

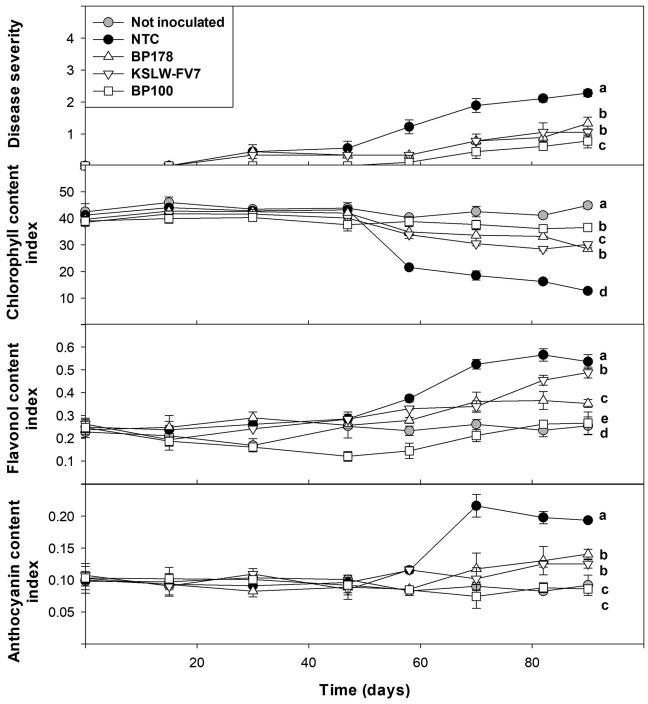

Fig. 7. Disease severity and leaf physiological parameters (chlorophyll, flavonol, and anthocyanin content index) of almond leaf scorch in plants inoculated with *X. fastidiosa* and treated with BP178, KSLW-FV7, and BP100 by endotherapy compared with a not-treated control (NTC) over a period of 90 days postinoculation. A not-inoculated control was added for reference for the leaf physiological parameters. For disease severity, values are the means of nine plants divided in three biological replicates. For the leaf physiological parameters, values are the means of four leaves/plant of a total of three biological replicates of three plants each. Error bars represent the confidence interval (α = 0.05). Different letters between treatments indicate significant overall differences between the treatments for each analyzed parameter according to Duncan's test ($P < 0.05$).

expression of type IV pili machinery regulatory genes, as described in other peptides (Huan et al. 2020). This is the case with the antimicrobial peptide Cec4, which inhibited twitching motility of *A. baumannii* by affecting the transcriptome profile of several type IV pili genes (Liu et al. 2020). Therefore, in a future work, it would be interesting to study in detail the mechanism of action of BP100 on the twitching motility of *X. fastidiosa*.

Finally, we demonstrated the protective effect BP100 in infected almond trees under greenhouse conditions, which showed lower disease severity symptoms and lower viable population levels of *X. fastidiosa* compared with the NTC. This protective effect was accompanied with leaf physiological parameter values similar to the not-inoculated plants. The reduction of population levels in BP100-treated plants could be mainly attributed to its effect on the twitching motility of *X. fastidiosa* because it did not show high bactericidal activity during the in vitro experiments, although the peptide may present some bactericidal and antibiofilm activity at the tested concentration in planta. Interestingly, population reduction was not statistically significant when compared with the other two peptides tested, BP178 and KSLW-FV7, that presented high bactericidal activity. Results obtained for BP178-treated plants are similar to those reported in a previous study regarding the reduction of disease severity and population levels when compared with the NTC (Moll et al. 2022). In addition, the population dynamics followed a similar pattern to that observed in a previous study (Baró et al. 2021). There was exponential growth until a maximum population level was

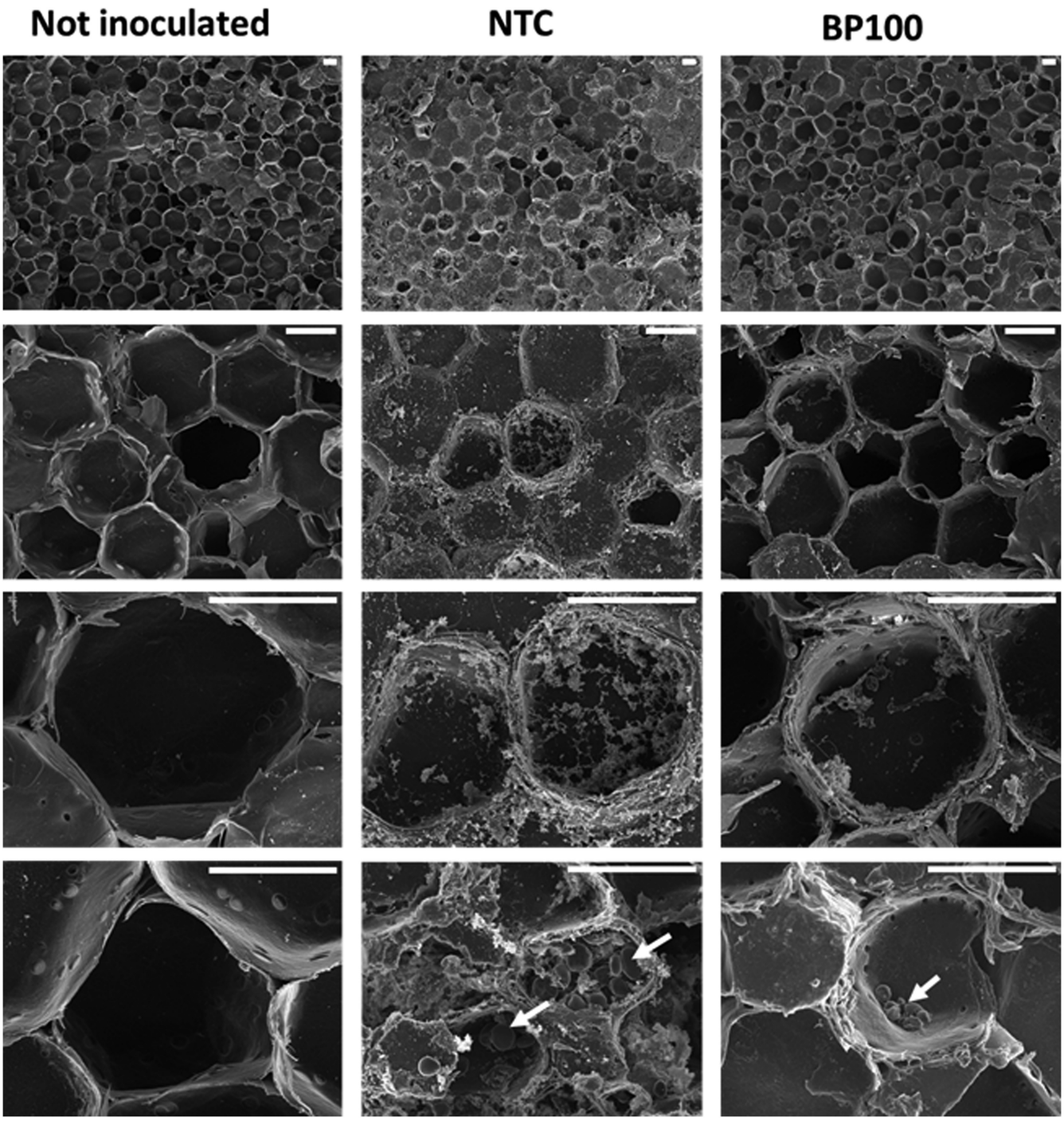

Fig. 8. Representative scanning electron micrographs of xylem vessels of *Prunus dulcis* plants that were not inoculated, inoculated with *X. fastidiosa* (not-treated control [NTC]), or inoculated with *X. fastidiosa* and treated with the peptide BP100. The white scale bar corresponds to 20 μm in all of the images. White arrows indicate tyloses formation.

reached, followed by exponential decrease, which corresponded to an exacerbation of disease symptoms. These observations are consistent with the predicted model for plant colonization by *X. fastidiosa*, which describes a first phase of systemic spread and multiplication followed by a second phase in which cells start to become locally abundant and stickier to the xylem vessels (Chatterjee et al. 2008a).

Regarding symptoms development and its associated leaf physiological parameters, BP100 displayed the best results among the other peptides. In the literature, it has been stated that the reduction of motility of *X. fastidiosa* reduces its colonization capability, slowing down the potential death of the host and resulting in higher chances of being acquired by an insect vector and transmitted to other plants (Guilhabert and Kirkpatrick 2005; Ionescu et al. 2014; Redak et al. 2004; Roper et al. 2019). This has been supported by experiments that restricted the motility of the pathogen by using diffusible signal factors or mutating specific genes (Chen et al. 2017; Cursino et al. 2009, 2011; Lindow et al. 2014; Shi and Lin 2018). Likewise, because BP100 affects the motility of *X. fastidiosa*, it may be partially keeping the bacterium in a sessile state that results in the lower disease severity observed. This is further supported by the leaf physiological parameters, in which the values obtained for the BP100-treated plants are similar to the not-inoculated ones. For example, the NTC showed higher values of flavonol and anthocyanin content compared with the BP100-treated plants, which are associated with higher stress levels (Camino et al. 2021; Purcino et al. 2007; Zarco-Tejada et al. 2018). These observations correlate with the lower frequency of affected xylem vessels found in BP100-treated plants when compared with the NTC, which are similar to the reduction of total occlusions found in the tolerant *Olea europea* cultivar Leccino when compared with the susceptible cultivars Ogliarola salentina and Cellina di Nardò (De Benedictis et al. 2017). Similar observations regarding the correlation of occlusion of xylem vessels by tyloses formation and symptoms were obtained with grapevine (Ingel et al. 2021).

As far as we know, the general mechanism of action of BP100 consists of the electrostatic interaction with the negatively charged membrane of the pathogen, which confers the peptide with some bactericidal and antibiofilm activity (Riesco-Llach et al. 2024). In addition, it has other properties, such as being a cell-penetrating peptide in eukaryotic cell models (Eggenberger et al. 2011). In this study, we demonstrated that BP100 is able to inhibit the motility of *X. fastidiosa* at low concentration, although the mechanism has yet to be elucidated. We also showed that BP100 has a protective effect in infected almond plants under greenhouse conditions, which could be attributed mostly to the inhibition of twitching motility. Nevertheless, it has to be considered that there might be some other mechanisms that have not been studied in this work that could be playing a role in the protective effect of BP100, such as the activation of the plant defense response. Therefore, the mechanism of action of BP100 in planta should be studied in detail in the future.

We report, for the first time, synthetic peptides that are able to reduce the twitching motility of *X. fastidiosa* on agar plate colonies and in cells under microfluidic chamber conditions. The most active peptide was BP100, and its protective effect in infected almond plants under greenhouse conditions has been demonstrated. BP100 could be a promising candidate to manage diseases, such as ALS, caused by *X. fastidiosa*.

Acknowledgments

The authors acknowledge the Serveis Tècnics de Recerca of the University of Girona (Spain) for the mass spectrometry analysis, and we thank Dr. Ester Marco from IVIA (Spain) for providing some of the *X. fastidiosa* strains. We are thankful for the support provided by Deepak Shantharaj, Ranlin Liu, and Noel Claudio during the twitching motility experiments performed at Auburn University. We thank Blanca Beatriz Landa and Miguel Román-Écija for their support in the TEM experiments that were performed at the electron microscopy facilities of the Central Research Support Services of the University of Córdoba (UCO-SCAI, Spain). We also thank Gemma Roselló, Hector Saravia, and Josep Antoni Pereda for participating in various tasks during the preparation and maintenance of plant material. Finally, we would like to thank Daniel Reyes from the Serveis Tècnics de Recerca of the University of Girona (Spain) for his support during the SEM experiments.

Literature Cited

AAT Bioquest. 2024. EC50 Calculator. https://www.aatbio.com/tools/ec50-calculator

Ajish, C., Kumar, S. D., Kim, E. Y., Yang, S., and Shin, S. Y. 2022. A short novel antimicrobial peptide BP100-W with antimicrobial, antibiofilm and anti-inflammatory activities designed by replacement with tryptophan. J. Anal. Sci. Technol. 13:46.

Alston, J. M., Fuller, K. B., Kaplan, J. D., and Tumber, K. P. 2013. Economic consequences of Pierce's disease and related policy in the California winegrape industry. J. Agric. Resour. Econ. 38:269-297.

Amanifar, N., Taghavi, M., and Salehi, M. 2016. *Xylella fastidiosa* from almond in Iran: Overwinter recovery and effects of antibiotics. Phytopathol. Mediterr. 55:337-345.

Anita, S., Capasso, V., Montagna, M., and Scacchi, S. 2022. Predators as a possible strategy for controlling a *Xylella* epidemic? Math. Model. Nat. Phenom. 17:42.

Avosani, S., Nieri, R., Mazzoni, V., Anfora, G., Hamouche, Z., Zippari, C., Vitale, M. L., Verrastro, V., Tarasco, E., D'Isita, I., Germinara, S., Döring, T. F., Belusic, G., Fereres, A., Thompson, V., and Cornara, D. 2024. Intruding into a conversation: How behavioral manipulation could support management of *Xylella fastidiosa* and its insect vectors. J. Pest Sci. 97:17-33.

Baccari, C., Antonova, E., and Lindow, S. 2019. Biological control of Pierce's disease of grape by an endophytic bacterium. Phytopathology 109:248-256.

Badosa, E., Ferre, R., Planas, M., Feliu, L., Besalú, E., Cabrefiga, J., Bardají, E., and Montesinos, E. 2007. A library of linear undecapeptides with bactericidal activity against phytopathogenic bacteria. Peptides 28:2276-2285.

Badosa, E., Planas, M., Feliu, L., Montesinos, L., Bonaterra, A., and Montesinos, E. 2022. Synthetic peptides against plant pathogenic bacteria. Microorganisms 10:1784.

Baró, A., Badosa, E., Montesinos, L., Feliu, L., Planas, M., Montesinos, E., and Bonaterra, A. 2020a. Screening and identification of BP100 peptide conjugates active against *Xylella fastidiosa* using a viability-qPCR method. BMC Microbiol. 20:229.

Baró, A., Montesinos, L., Badosa, E., and Montesinos, E. 2021. Aggressiveness of Spanish isolates of *Xylella fastidiosa* to almond plants of different cultivars under greenhouse conditions. Phytopathology 111:1994-2001.

Baró, A., Mora, I., Montesinos, L., and Montesinos, E. 2020b. Differential susceptibility of *Xylella fastidiosa* strains to synthetic bactericidal peptides. Phytopathology 110:1018-1026.

Beaulieu, E. D., Ionescu, M., Chatterjee, S., Yokota, K., Trauner, D., and Lindow, S. 2013. Characterization of a diffusible signaling factor from *Xylella fastidiosa*. mBio 4:e00539-12.

Burbank, L. P. 2022. Threat of *Xylella fastidiosa* and options for mitigation in infected plants. CABI Rev. https://doi.org/10.1079/cabireviews202217021

Camino, C., Calderón, R., Parnell, S., Dierkes, H., Chemin, Y., Román-Écija, M., Montes-Borrego, M., Landa, B. B., Navas-Cortes, J. A., Zarco-Tejada, P. J., and Beck, P. S. A. 2021. Detection of *Xylella fastidiosa* in almond orchards by synergic use of an epidemic spread model and remotely sensed plant traits. Remote Sens. Environ. 260:112420.

Camó, C., Bonaterra, A., Badosa, E., Baró, A., Montesinos, L., Montesinos, E., Planas, M., and Feliu, L. 2019. Antimicrobial peptide KSL-W and analogues: Promising agents to control plant diseases. Peptides 112:85-95.

Caravaca-Fuentes, P., Camó, C., Oliveras, À., Baró, A., Francés, J., Badosa, E., Planas, M., Feliu, L., Montesinos, E., and Bonaterra, A. 2021. A bifunctional peptide conjugate that controls infections of *Erwinia amylovora* in pear plants. Molecules 26:3426.

Cardinale, M., Luvisi, A., Meyer, J. B., Sabella, E., De Bellis, L., Cruz, A. C., Ampatzidis, Y., and Cherubini, P. 2018. Specific fluorescence *in situ* hybridization (FISH) test to highlight colonization of xylem vessels by *Xylella fastidiosa* in naturally infected olive trees (*Olea europaea* L.). Front. Plant Sci. 9:431.

Carluccio, G., Greco, D., Sabella, E., Vergine, M., De Bellis, L., and Luvisi, A. 2023. Xylem embolism and pathogens: Can the vessel anatomy of woody plants contribute to *X. fastidiosa* resistance? Pathogens 12:825.

Cerovic, Z. G., Masdoumier, G., Ghozlen, N. B., and Latouche, G. 2012. A new optical leaf-clip meter for simultaneous non-destructive assessment of leaf chlorophyll and epidermal flavonoids. Physiol. Plant. 146:251-260.

Chatterjee, S., Almeida, R. P. P., and Lindow, S. 2008a. Living in two worlds: The plant and insect lifestyles of *Xylella fastidiosa*. Annu. Rev. Phytopathol. 46: 243-271.

Chatterjee, S., Killiny, N., Almeida, R. P. P., and Lindow, S. E. 2010. Role of cyclic di-GMP in *Xylella fastidiosa* biofilm formation, plant virulence, and insect transmission. Mol. Plant-Microbe Interact. 23:1356-1363.

Chatterjee, S., Newman, K. L., and Lindow, S. E. 2008b. Cell-to-cell signaling in *Xylella fastidiosa* suppresses movement and xylem vessel colonization in grape. Mol. Plant-Microbe Interact. 21:1309-1315.

Chatterjee, S., Wistrom, C., and Lindow, S. E. 2008c. A cell–cell signaling sensor is required for virulence and insect transmission of *Xylella fastidiosa*. Proc. Natl. Acad. Sci. U.S.A. 105:2670-2675.

Chen, H., and De La Fuente, L. 2020. Calcium transcriptionally regulates movement, recombination and other functions of *Xylella fastidiosa* under constant flow inside microfluidic chambers. Microb. Biotechnol. 13:548-561.

Chen, H., Kandel, P. P., Cruz, L. F., Cobine, P. A., and De La Fuente, L. 2017. The major outer membrane protein MopB is required for twitching movement and affects biofilm formation and virulence in two *Xylella fastidiosa* strains. Mol. Plant-Microbe Interact. 30:896-905.

Choueiri, E., Abou Kubaa, R., Valentini, F., Yaseen, T., El Sakka, H., Gerges, S., La Notte, P., Saponari, M., Elbeaino, T., and El Moujabber, M. 2023. First report of *Xylella fastidiosa* on almond (*Prunus dulcis*) in Lebanon. J. Plant Pathol. 105:1157.

Cobine, P. A., Cruz, L. F., Navarrete, F., Duncan, D., Tygart, M., and De La Fuente, L. 2013. *Xylella fastidiosa* differentially accumulates mineral elements in biofilm and planktonic cells. PLoS One 8:e54936.

Craig, L., Forest, K. T., and Maier, B. 2019. Type IV pili: Dynamics, biophysics and functional consequences. Nat. Rev. Microbiol. 17:429-440.

Cruz, L. F., Cobine, P. A., and De La Fuente, L. 2012. Calcium increases *Xylella fastidiosa* surface attachment, biofilm formation, and twitching motility. Appl. Environ. Microbiol. 78:1321-1331.

Cruz, L. F., Parker, J. K., Cobine, P. A., and De La Fuente, L. 2014. Calcium-enhanced twitching motility in *Xylella fastidiosa* is linked to a single PilY1 homolog. Appl. Environ. Microbiol. 80:7176-7185.

Cursino, L., Galvani, C. D., Athinuwat, D., Zaini, P. A., Li, Y., De La Fuente, L., Hoch, H. C., Burr, T. J., and Mowery, P. 2011. Identification of an operon, Pil-Chp, that controls twitching motility and virulence in *Xylella fastidiosa*. Mol. Plant-Microbe Interact. 24:1198-1206.

Cursino, L., Li, Y., Zaini, P. A., De La Fuente, L., Hoch, H. C., and Burr, T. J. 2009. Twitching motility and biofilm formation are associated with *tonB1* in *Xylella fastidiosa*. FEMS Microbiol. Lett. 299:193-199.

Das, M., Bhowmick, T. S., Ahern, S. J., Young, R., and Gonzalez, C. F. 2015. Control of Pierce's disease by phage. PLoS One 10:e0128902.

D'Attoma, G., Morelli, M., De La Fuente, L., Cobine, P. A., Saponari, M., de Souza, A. A., De Stradis, A., and Saldarelli, P. 2020. Phenotypic characterization and transformation attempts reveal peculiar traits of *Xylella fastidiosa* subspecies *pauca* strain De Donno. Microorganisms 8:1832.

Davis, M. J., French, W. J., and Schaad, N. W. 1981. Axenic culture of the bacteria associated with phony disease of peach and plum leaf scald. Curr. Microbiol. 6: 309-314.

Davis, M. J., Purcell, A. H., and Thomson, S. V. 1980. Isolation media for the Pierce's disease bacterium. Phytopathology 70:425-429.

De Benedictis, M., De Caroli, M., Baccelli, I., Marchi, G., Bleve, G., Gallo, A., Ranaldi, F., Falco, V., Pasquali, V., Piro, G., Mita, G., and Di Sansebastiano, G. P. 2017. Vessel occlusion in three cultivars of *Olea europaea* naturally exposed to *Xylella fastidiosa* in open field. J. Phytopathol. 165:589-594.

De La Fuente, L., Burr, T. J., and Hoch, H. C. 2007a. Mutations in type I and type IV pilus biosynthetic genes affect twitching motility rates in *Xylella fastidiosa*. J. Bacteriol. 189:7507-7510.

De La Fuente, L., Montanes, E., Meng, Y., Li, Y., Burr, T. J., Hoch, H. C., and Wu, M. 2007b. Assessing adhesion forces of type I and type IV pili of *Xylella fastidiosa* bacteria by use of a microfluidic flow chamber. Appl. Environ. Microbiol. 73:2690-2696.

de la Fuente-Núñez, C., Korolik, V., Bains, M., Nguyen, U., Breidenstein, E. B. M., Horsman, S., Lewenza, S., Burrows, L., and Honcock, R. E. W. 2012. Inhibition of bacterial biofilm formation and swarming motility by a small synthetic cationic peptide. Antimicrob. Agents Chemother. 56:2696-2704.

de la Fuente-Núñez, C., Reffuveille, F., Mansour, S. C., Reckseidler-Zenteno, S. L., Hernández, D., Brackman, G., Coenye, T., and Hancock, R. E. W. 2015. D-Enantiomeric peptides that eradicate wild-type and multidrug-resistant biofilms and protect against lethal *Pseudomonas aeruginosa* infections. Chem. Biol. 22:196-205.

Dong, N., Wang, C., Zhang, T., Zhang, L., Xue, C., Feng, X., Bi, C., and Shan, A. 2019. Bioactivity and bactericidal mechanism of histidine-rich β-hairpin peptide against gram-negative bacteria. Int. J. Mol. Sci. 20:3954.

Dunger, G., Llontop, E., Guzzo, C. R., and Farah, C. S. 2016. The *Xanthomonas* type IV pilus. Curr. Opin. Microbiol. 30:88-97.

EFSA Panel on Plant Health (EFSA PLH Panel), Jeger, M., Caffier, D., Candresse, T., Chatzivassiliou, E., Dehnen-Schmutz, K., Gilioli, G., Grégoire, J.-C., Jaques Miret, J. A., MacLeod, A., Navarro, M. N., Niere, B., Parnell, S., Potting, R., Rafoss, T., Rossi, V., Urek, G., Van Bruggen, A., Van der Werf, W., West, J., Winter, S., Almeida, R., Bosco, D., Jacques, M.-A., Landa, B., Purcell, A., Saponari, M., Czwienczek, E., Delbianco, A., Stancanelli, G., and Bragard, C. 2018. Updated pest categorisation of *Xylella fastidiosa*. EFSA J. 16:e05357.

EFSA Panel on Plant Health (EFSA PLH Panel), Bragard, C., Dehnen-Schmutz, K., Di Serio, F., Gonthier, P., Jacques, M.-A., Jaques Miret, J. A., Justesen, A. F., MacLeod, A., Magnusson, C. S., Milonas, P., Navas-Cortés, J. A., Potting, R., Reignault, P. L., Thulke, H.-H., Van der Werf, W., Civera, A. V., Yuen, J., Zappalà, L., Makowski, D., Delbianco, A., Maiorano, A., Guajardo, I. M., Stancanelli, G., Guzzo, M., and Parnell, S. 2019. Effectiveness of in planta control measures for *Xylella fastidiosa.* EFSA J. 17:e05666.

Eggenberger, K., Mink, C., Wadhwani, P., Ulrich, A. S., and Nick, P. 2011. Using the peptide Bp100 as a cell-penetrating tool for the chemical engineering of actin filaments within living plant cells. ChemBioChem 12:132-137.

European and Mediterranean Plant Protection Organization (EPPO). 2006. Intentional import of organisms that are plant pests or potential plant pests. EPPO Bull. 36:191-194.

European Food Safety Authority. 2013. Statement of EFSA on host plants, entry and spread pathways and risk reduction options for *Xylella fastidiosa* Wells et al. EFSA J. 11:3468.

European Food Safety Authority (EFSA), Gibin, D., Gutierrez Linares, A., Fasanelli, E., Pasinato, L., and Delbianco, A. 2023. Update of the *Xylella* spp. host plant database – systematic literature search up to 30 June 2023. EFSA J. 21:e8477.

European Union. 2019. Commission Implementing Regulation (EU) 2019/2072 of 28 November 2019 establishing uniform conditions for the implementation of Regulation (EU) 2016/2031 of the European Parliament and the Council, as regards protective measures against pests of plants, and repealing Commission Regulation (EC) No 690/2008 and amending Commission Implementing Regulation (EU) 2018/2019. 1-279. http://data.europa.eu/eli/reg_impl/2019/2072/oj

European Union. 2020. Commission Implementing Regulation (EU) 2020/1201 of 14 August 2020 as regards measures to prevent the introduction into and the spread within the Union of *Xylella fastidiosa* (Wells et al.). O.J. (L 269) 17.8.2020:2–39. http://data.europa.eu/eli/reg_impl/2020/1201/oj

European Union. 2021. Commission Implementing Regulation (EU) 2021/2285 of 14 December 2021 amending Implementing Regulation (EU) 2019/2072 as regards the listing of pests, prohibitions and requirements for the introduction into, and movement within, the Union of plants, plant products and other objects, and repealing Decisions 98/109/EC and 2002/757/EC and Implementing Regulations (EU) 2020/885 and (EU) 2020/1292. 173-283. http://data.europa.eu/eli/reg_impl/2021/2285/oj

Fogaça, A. C., Zaini, P. A., Wulff, N. A., Da Silva, P. I. P., Fázio, M. A., Miranda, A., Daffre, S., and Da Silva, A. M. 2010. Effects of the antimicrobial peptide gomesin on the global gene expression profile, virulence and biofilm formation of *Xylella fastidiosa*. FEMS Microbiol. Lett. 306:152-159.

Galvani, C. D., Li, Y., Burr, T. J., and Hoch, H. C. 2007. Twitching motility among pathogenic *Xylella fastidiosa* isolates and the influence of bovine serum albumin on twitching-dependent colony fringe morphology. FEMS Microbiol. Lett. 268: 202-208.

Gawande, P. V., Leung, K. P., and Madhyastha, S. 2014. Antibiofilm and antimicrobial efficacy of DispersinB®-KSL-W peptide-based wound gel against chronic wound infection associated bacteria. Curr. Microbiol. 68:635-641.

Ge, Q., Cobine, P. A., and De La Fuente, L. 2020. Copper supplementation in watering solution reaches the xylem but does not protect tobacco plants against *Xylella fastidiosa* infection. Plant Dis. 104:724-730.

Guilhabert, M. R., and Kirkpatrick, B. C. 2005. Identification of *Xylella fastidiosa* antivirulence genes: Hemagglutinin adhesins contribute to *X. fastidiosa* biofilm maturation and colonization and attenuate virulence. Mol. Plant-Microbe Interact. 18:856-868.

Hao, L., Johnson, K., Cursino, L., Mowery, P., and Burr, T. J. 2017. Characterization of the *Xylella fastidiosa* PD1311 gene mutant and its suppression of Pierce's disease on grapevines. Mol. Plant Pathol. 18:684-694.

Horn, M., and Neundorf, I. 2018. Design of a novel cell-permeable chimeric peptide to promote wound healing. Sci. Rep. 8:16279.

Huan, Y., Kong, Q., Mou, H., and Yi, H. 2020. Antimicrobial peptides: Classification, design, application and research progress in multiple fields. Front. Microbiol. 11:582779.

Ingel, B., Reyes, C., Massonnet, M., Boudreau, B., Sun, Y., Sun, Q., McElrone, A. J., Cantu, D., and Roper, M. C. 2021. *Xylella fastidiosa* causes transcriptional shifts that precede tylose formation and starch depletion in xylem. Mol. Plant Pathol. 22: 175-188.

Ionescu, M., Zaini, P. A., Baccari, C., Tran, S., da Silva, A. M., and Lindow, S. E. 2014. *Xylella fastidiosa* outer membrane vesicles modulate plant colonization by blocking attachment to surfaces. Proc. Natl. Acad. Sci. U.S.A. 111: E3910-E3918.

Jacobsen, T., Bardiaux, B., Francetic, O., Izadi-Pruneyre, N., and Nilges, M. 2020. Structure and function of minor pilins of type IV pili. Med. Microbiol. Immunol. 209:301-308.

Kaiser, D. 2000. Bacterial motility: How do pili pull? Curr. Biol. 10:R777-R780.

Kim, M. K., Kang, H. K., Ko, S. J., Hong, M. J., Bang, J. K., Seo, C. H., and Park, Y. 2018. Mechanisms driving the antibacterial and antibiofilm properties of Hp1404 and its analogue peptides against multidrug-resistant *Pseudomonas aeruginosa*. Sci. Rep. 8:1763.

Kumar, L., Chhibber, S., and Harjai, K. 2013. Zingerone inhibit biofilm formation and improve antibiofilm efficacy of ciprofloxacin against *Pseudomonas aeruginosa* PAO1. Fitoterapia 90:73-78.

Kuzina, L. V., Miller, T. A., and Cooksey, D. A. 2006. In vitro activities of antibiotics and antimicrobial peptides against the plant pathogenic bacterium *Xylella fastidiosa*. Lett. Appl. Microbiol. 42:514-520.

Li, Y., Hao, G., Galvani, C. D., Meng, Y., De La Fuente, L., Hoch, H. C., and Burr, T. J. 2007. Type I and type IV pili of *Xylella fastidiosa* affect twitching motility, biofilm formation and cell–cell aggregation. Microbiology 153:719-726.

Li, Z. T., and Gray, D. J. 2003. Effect of five antimicrobial peptides on the growth of *Agrobacterium tumefaciens, Escherichia coli* and *Xylella fastidiosa*. Vitis 42:95-97.

Lindow, S., Koutsoukis, R., Meyer, K., and Baccari, C. 2024. Control of Pierce's disease of grape with *Paraburkholderia phytofirmans* PsJN in the field. Phytopathology 114:503-511.

Lindow, S., Newman, K., Chatterjee, S., Baccari, C., Lavarone, A. T., and Ionescu, M. 2014. Production of *Xylella fastidiosa* diffusible signal factor in transgenic grape causes pathogen confusion and reduction in severity of Pierce's disease. Mol. Plant-Microbe Interact. 27:244-254.

Liu, W., Wu, Z., Mao, C., Guo, G., Zeng, Z., Fei, Y., Wan, S., Peng, J., and Wu, J. 2020. Antimicrobial peptide Cec4 eradicates the bacteria of clinical carbapenem-resistant *Acinetobacter baumannii* biofilm. Front. Microbiol. 11: 1532.

Matsumoto, G. O., Febres, V. J., Harmon, P. F., and Chaparro, J. X. 2023. Survey of *Xylella fastidiosa* infection in *Prunus* germplasm in Gainesville, FL, USA. HortScience 58:819-824.

Meng, Y., Li, Y., Galvani, C. D., Hao, G., Turner, J. N., Burr, T. J., and Hoch, H. C. 2005. Upstream migration of *Xylella fastidiosa* via pilus-driven twitching motility. J. Bacteriol. 187:5560-5567.

Merfa, M. V., Zhu, X., Shantharaj, D., Gomez, L. M., Naranjo, E., Potnis, N., Cobine, P. A., and De La Fuente, L. 2023. Complete functional analysis of type IV pilus components of a reemergent plant pathogen reveals neofunctionalization of paralog genes. PLoS Pathog. 19:e1011154.

Moll, L., Badosa, E., Planas, M., Feliu, L., Montesinos, E., and Bonaterra, A. 2021. Antimicrobial peptides with antibiofilm activity against *Xylella fastidiosa*. Front. Microbiol. 12:753874.

Moll, L., Baró, A., Montesinos, L., Badosa, E., Bonaterra, A., and Montesinos, E. 2022. Induction of defense responses and protection of almond plants against *Xylella fastidiosa* by endotherapy with a bifunctional peptide. Phytopathology 112:1907-1916.

Montesinos, E. 2023. Functional peptides for plant disease control. Annu. Rev. Phytopathol. 61:301-324.

Montesinos, L., Gascón, B., Ruz, L., Badosa, E., Planas, M., Feliu, L., and Montesinos, E. 2021. A bifunctional synthetic peptide with antimicrobial and plant elicitation properties that protect tomato plants from bacterial and fungal infections. Front. Plant Sci. 12:756357.

Muranaka, L. S., Giorgiano, T. E., Takita, M. A., Forim, M. R., Silva, L. F. C., Coletta-Filho, H. D., Machado, M. A., and de Souza, A. A. 2013. N-Acetylcysteine in agriculture, a novel use for an old molecule: Focus on controlling the plant-pathogen *Xylella fastidiosa*. PLoS One 8:e72937.

Na, D. H., Faraj, J., Capan, Y., Leung, K. P., and DeLuca, P. P. 2007. Stability of antimicrobial decapeptide (KSL) and its analogues for delivery in the oral cavity. Pharm. Res. 24:1544-1550.

Nadal, A., Montero, M., Company, N., Badosa, E., Messeguer, J., Montesinos, L., Montesinos, E., and Pla, M. 2012. Constitutive expression of transgenes encoding derivatives of the synthetic antimicrobial peptide BP100: Impact on rice host plant fitness. BMC Plant Biol. 12:159.

Oliveras, À., Camó, C., Caravaca-Fuentes, P., Moll, L., Riesco-Llach, G., Gil-Caballero, S., Badosa, E., Bonaterra, A., Montesinos, E., Feliu, L., and Planas, M. 2022. Peptide conjugates derived from flg15, Pep13, and PIP1 that are active against plant-pathogenic bacteria and trigger plant defense responses. Appl. Environ. Microbiol. 88:e00574-22.

Oliveras, À., Moll, L., Riesco-Llach, G., Tolosa-Canudas, A., Gil-Caballero, S., Badosa, E., Bonaterra, A., Montesinos, E., Planas, M., and Feliu, L. 2021. D-Amino acid-containing lipopeptides derived from the lead peptide BP100 with activity against plant pathogens. Int. J. Mol. Sci. 22:6631.

Pereira, W. E. L., Ferreira, C. B., Caserta, R., Melotto, M., and de Souza, A. A. 2019. *Xylella fastidiosa* subsp. *pauca* and *fastidiosa* colonize *Arabidopsis* systemically and induce anthocyanin accumulation in infected leaves. Phytopathology 109: 225-232.

Purcell, A. 2013. Paradigms: Examples from the bacterium *Xylella fastidiosa*. Annu. Rev. Phytopathol. 51:339-356.

Purcino, R. P., Medina, C. L., Martins de Souza, D., Winck, F. V., Machado, E. C., Novello, J. C., Machado, M. A., and Mazzafera, P. 2007. *Xylella fastidiosa* disturbs nitrogen metabolism and causes a stress response in sweet orange *Citrus sinensis* cv. Pêra. J. Exp. Bot. 58:2733-2744.

Raheem, N., and Straus, S. K. 2019. Mechanisms of action for antimicrobial peptides with antibacterial and antibiofilm functions. Front. Microbiol. 10:2866.

Rapicavoli, J., Ingel, B., Blanco-Ulate, B., Cantu, D., and Roper, C. 2018. *Xylella fastidiosa*: An examination of a re-emerging plant pathogen. Mol. Plant Pathol. 19:786-800.

Redak, R. A., Purcell, A. H., Lopes, J. R. S., Blua, M. J., Mizell, R. F., III, and Andersen, P. C. 2004. The biology of xylem fluid-feeding insect vectors of *Xylella fastidiosa* and their relation to disease epidemiology. Annu. Rev. Entomol. 49:243-270.

Riesco-Llach, G., Llanet-Ferrer, S., Planas, M., and Feliu, L. 2024. Deciphering the mechanism of action of the antimicrobial peptide BP100. Int. J. Mol. Sci. 25:3456.

Román-Écija, M., Navas-Cortés, J. A., Velasco-Amo, M. P., Arias-Giraldo, L. F., Gómez, L. M., De La Fuente, L., and Landa, B. B. 2023. Two *Xylella fastidiosa* subsp. *multiplex* strains isolated from almond in Spain differ in plasmid content and virulence traits. Phytopathology 113:960-974.

Roper, C., Castro, C., and Ingel, B. 2019. *Xylella fastidiosa*: Bacterial parasitism with hallmarks of commensalism. Curr. Opin. Plant Biol. 50:140-147.

Sánchez, B., Barreiro-Hurle, J., Soto Embodas, I., and Rodriguez-Cerezo, E. 2019. The Impact Indicator for Priority Pests (I2P2): A Tool for Ranking Pests According to Regulation (EU) No 2016/2031. Publications Office of the European Union, Luxembourg, Luxembourg. https://data.europa.eu/doi/10.2760/585182

Scala, V., Pucci, N., Salustri, M., Modesti, V., L'Aurora, A., Scortichini, M., Zaccaria, M., Momeni, B., Reverberi, M., and Loreti, S. 2020. *Xylella fastidiosa* subsp. *pauca* and olive produced lipids moderate the switch adhesive versus non-adhesive state and viceversa. PLoS One 15:e0233013.

Scortichini, M., Chen, J., de Caroli, M., Dalessandro, G., Pucci, N., Modesti, V., L'Aurora, A., Petriccione, M., Zampella, L., Mastrobuoni, F., Migoni, D., Del Coco, L., Girelli, C. R., Piacente, F., Cristella, N., Marangi, P., Laddomada, F., Di Cesare, M., Cesari, G., Fanizzi, F. P., and Loreti, S. 2018. A zinc, copper and citric acid biocomplex shows promise for control of *Xylella fastidiosa* subsp. *pauca* in olive trees in Apulia region (southern Italy). Phytopathol. Mediterr. 57:48-72.

Shang, D., Han, X., Du, W., Kou, Z., and Jiang, F. 2021. Trp-containing antibacterial peptides impair quorum sensing and biofilm development in multidrug-resistant *Pseudomonas aeruginosa* and exhibit synergistic effects with antibiotics. Front. Microbiol. 12:611009.

Shi, X., and Lin, H. 2016. Visualization of twitching motility and characterization of the role of the *pilG* in *Xylella fastidiosa*. J. Vis. Exp. 110:53816.

Shi, X., and Lin, H. 2018. The chemotaxis regulator *pilG* of *Xylella fastidiosa* is required for virulence in *Vitis vinifera* grapevines. Eur. J. Plant Pathol. 150:351-362.

Stefani, E., Obradović, A., Gašić, K., Altin, I., Nagy, I. K., and Kovács, T. 2021. Bacteriophage-mediated control of phytopathogenic xanthomonads: A promising green solution for the future. Microorganisms 9:1056.

Strona, G., Carstens, C. J., and Beck, P. S. A. 2017. Network analysis reveals why *Xylella fastidiosa* will persist in Europe. Sci. Rep. 7:71.

Wells, J. M., Raju, B. C., Nyland, G., and Lowe, S. K. 1981. Medium for isolation and growth of bacteria associated with plum leaf scald and phony peach diseases. Appl. Environ. Microbiol. 42:357-363.

Xu, W., Zhu, X., Tan, T., Li, W., and Shan, A. 2014. Design of embedded-hybrid antimicrobial peptides with enhanced cell selectivity and anti-biofilm activity. PLoS One 9:e98935.

Yilmaz, N., Kodama, Y., and Numata, K. 2021. Lipid membrane interaction of peptide/DNA complexes designed for gene delivery. Langmuir 37: 1882-1893.

Zarco-Tejada, P. J., Camino, C., Beck, P. S. A., Calderon, R., Hornero, A., Hernández-Clemente, R., Kattenborn, T., Montes-Borrego, M., Susca, L., Morelli, M., Gonzalez-Dugo, V., North, P. R. J., Landa, B. B., Boscia, D., Saponari, M., and Navas-Cortes, J. A. 2018. Previsual symptoms of *Xylella fastidiosa* infection revealed in spectral plant-trait alterations. Nat. Plants 4: 432-439.